Chrna5 is a marker of acetylcholine super-responder subplate neurons with specialized expression of nicotinic modulator proteins

Sridevi Venkatesan[1], Tianhui Chen[1], Yupeng Liu[1], Eric E Turner[2], Shreejoy Tripathy[1,3,4,5], *Evelyn K Lambe[1,4,6]

1. Department of Physiology, Temerty Faculty of Medicine, University of Toronto, Toronto ON, Canada
2. Center for Integrative Brain Research, Seattle Children's Research Institute, Seattle WA, USA
3. Krembil Centre for Neuroinformatics, Centre for Addiction and Mental Health, Toronto ON, Canada
4. Department of Psychiatry, University of Toronto, Toronto ON, Canada
5. Institute of Medical Science, University of Toronto, Toronto ON, Canada
6. Department of Obstetrics and Gynecology, University of Toronto, Toronto ON, Canada

Corresponding author:
E.K. Lambe, Ph.D.
1 King's College Circle
Toronto ON
Canada M5S 1A8
(416) 946-0910
Email: evelyn.lambe@utoronto.ca

Pages: 34
Figures: 9
Tables: 1
Supplementary materials: 5
Words: Abstract (150), Introduction (609), Discussion (1106)

Conflicts of interest: None

Acknowledgements: We acknowledge the generous support of the Canadian Institutes of Health Research (CIHR MOP 89825, EKL; CIHR PJT-153101, EKL), the Canada Research Chair in Developmental Cortical Physiology (EKL), an Ontario Graduate Scholarship (SV). We thank Ms. Janice McNabb and Mr. Ha-Seul Jeoung for expert technical assistance. Earlier presentations of this work received valuable feedback from Dr. Junchul Kim, Dr. Beverly Orser, and Dr. Steve Prescott of the University of Toronto.

Abstract (150 words)

Attention depends on cholinergic excitation of prefrontal neurons. Knockout/knockdown studies indicate nicotinic alpha5 subunits encoded by *Chrna5* are required for this response, but their native cellular roles and molecular interactions are unknown. Here, we probe endogenous cholinergic regulation of prefrontal *Chrna5*-expressing neurons (Chrna5+) using compound transgenic mice. Chrna5+ neurons show high sensitivity to acetylcholine, with a subpopulation clearly different from nearby, well-examined Syt6+ cells. Transcriptomic analysis reveals this distinct Chrna5+ population as subplate neurons, a diverse group of firstborn cells that have eluded previous transgenic characterization. Intriguingly, Chrna5+ subplate neurons express a distinct profile of GPI-anchored lynx prototoxins, suggesting specialized regulation of their cholinergic responses. In brain slices, endogenous nicotinic responses can be bidirectionally altered by perturbing GPI-anchored lynxes with phospholipase C activation or exogenous application of recombinant Ly6g6e prototoxin. Our work reveals cell-type specific *Chrna5* and Lynx modulation leading to exquisite cholinergic sensitivity of prefrontal subplate neurons in adulthood.

Teaser

Chrna5-expression identifies subplate neurons in the adult prefrontal cortex with enhanced cholinergic sensitivity.

Introduction (609 words)

Cholinergic modulation of the medial prefrontal cortex (mPFC) is essential for attention and detection of sensory cues (*1–4*). Deep-layer pyramidal neurons in the PFC are critically involved in such executive function (*5–7*) and are robustly excited by acetylcholine (*8*, *9*), through nicotinic and muscarinic receptor activation (*10*). The α5 nicotinic receptor subunit encoded by *Chrna5* is specifically expressed in deep-layer pyramidal neurons (*11*, *12*), forming high-affinity nicotinic receptors in combination with α4 and β2 subunits. Electrophysiological, behavioural, and genetic evidence in both rodents and humans point to an important role of *Chrna5* expression for nicotinic receptor function, attention, and executive function.

Constitutive knock out of *Chrna5* in mice or knockdown in the adult rat PFC disrupts attention and reduce nicotinic receptor activation by exogenous acetylcholine stimulation in layer 6 neurons (*13–15*). Optogenetic experiments in *Chrna5*$^{-/-}$ mice show that *Chrna5* is required for rapid onset of postsynaptic cholinergic activation and prevents desensitization of the endogenous cholinergic response during prolonged stimulation (*16*). In humans, the non-synonymous rs16969968 (D398N) polymorphism in *Chrna5* is associated with nicotine dependence, schizophrenia and cognitive impairment (*17–19*). Nicotinic α4β2α5 receptors with the D398N polymorphism have partial loss of function, attributed to changes in receptor desensitization, calcium permeability, or membrane trafficking (*20–22*).

Despite the clear indications of alpha5 nicotinic receptor involvement in attention and prefrontal cholinergic activation, systematic characterization of *Chrna5*-expressing neurons using modern genetic tools is lacking. Deep-layer neurons include diverse corticothalamic (L6CT), corticocortical, and layer 6b (L6b) populations (*23–25*). *Chrna5* is predicted to be expressed in L6CT neurons (*8*, *26*), which are usually identified by their expression of *Syt6*, a conserved L6CT neuronal marker (*27–29*). *Syt6*-Cre mice have been widely used to characterize prefrontal L6CT neurons and their cholinergic properties (*30–32*). However, it is unclear whether these are the same neurons expressing *Chrna5*. Characterization of *Chrna5*-expressing neurons has been limited by the lack of verified antibodies for the α5 subunit that could be used for post-hoc immunostaining. Previous BAC-transgenic mice labeling *Chrna5*-expressing neurons had altered expression of other genes in the tightly linked *Chrna5/a3/b4* gene cluster, limiting their use for functional examination (*33*). This issue was circumvented by disrupting the open reading frames of *Chrna3/b4* in the BAC transgene to generate a *Chrna5*-Cre mouse without misexpression artifacts (*34*).

Using compound transgenic mice, we first interrogated the response to optogenetic cholinergic stimulation and found stronger and faster responses in prefrontal *Chrna5*-expressing (Chrna5+) versus nonlabelled neurons. This prompted multi-approach characterization of Chrna5+ neurons versus better-defined *Syt6*-expressing (Syt6+) neurons. A large subset of Chrna5+ neurons were dissimilar to Syt6+ neurons, demonstrating higher affinity acetylcholine responses. Single-cell RNAseq analysis revealed the expression of several subplate markers (*Cplx3*, *Ctgf*, and *Lpar1*) in this Chrna5+ subset, identifying them as subplate neurons born early in development that are critical for establishing thalamocortical connectivity (*35–37*). Chrna5+ subplate neurons had a distinct expression pattern of GPI-anchored Lynx prototoxins with significantly enhanced

expression of *Ly6g6e*, *Lypd1*, and *Lypd6b,* together capable of exerting complex modulation of nicotinic receptor properties (*38*, *39*). Consistently, removing GPI-anchored lynxes by PLC activation altered optogenetic nicotinic response onset and amplitude. Exogenous application of Ly6g6e prototoxin suppressed Syt6+ but not Chrna5+ nicotinic responses, revealing complex cell-type specific Lynx-mediated regulation of nicotinic receptors.

Recent studies have focused on cell-type specific modulation of nicotinic receptors by different Lynx prototoxins and the consequences for cortical development and cognition (*40–43*). Here, we discovered endogenous Lynx modulation of nicotinic properties relevant for attention in subplate neurons expressing *Chrna5*. These findings provide the first characterization of Chrna5+ neurons and the molecular determinants underlying their cholinergic properties, while identifying *Chrna5* as a marker for subplate neurons with greater cholinergic responses.

Methods

Animals

Syt6-Cre$^{/+}$GCaMP6s$^{/+}$ and *Chrna5*-Cre$^{/+}$GCaMP6s$^{/+}$ mice used for calcium imaging were obtained by crossing *Chrna5*-Cre (Gift from Dr. Eric Turner) and *Syt6*-Cre mice (*Syt6*-Cre KI148, RRID:MMRRC 037416-UCD, (*44*)) respectively, with Ai96 mice (JAX: 024106). For electrophysiological recordings of labeled Chrna5+ and Syt6+ neurons, we used *Chrna5*-Cre$^{/+}$Ai14$^{/+}$, and *Syt6*-Cre$^{/+}$Ai14$^{/+}$ mice respectively. *Syt6*-EGFP$^{/+}$ mice were additionally used for few experiments (*Syt6*-EGFP EL71, RRID:MMRRC 010557-UCD, (*45*)).

Triple transgenic mice labeling both *Chrna5* and *Syt6*-expressing neurons with EGFP in Syt6+ neurons and tdTomato in Chrna5+ neurons were used to examine the overlap between the two cell types. *Syt6*-EGFP and Ai14 mice (*46*) were bred together and the offspring were crossed with *Chrna5*-Cre mice to generate *Chrna5*-Cre$^{/+}$Ai14$^{/+}$*Syt6*-EGFP$^{/+}$ mice used for these experiments. A set of experiments measuring optogenetic cholinergic responses was also performed in ChAT-ChR2 (ChAT$^{/+}$) mice (JAX: 014546). To examine optogenetic cholinergic responses in labeled Chrna5 and Syt6 cell populations, the respective Cre lines were crossed with ChAT$^{/+}$Ai14$^{/+}$ mice to generate *Chrna5*-Cre$^{/+}$Ai14$^{/+}$ChAT$^{/+}$ and *Syt6*-Cre$^{/+}$Ai14$^{/+}$ChAT$^{/+}$ mice.

All animals were bred on a C57BL/6 background, except *Syt6*-EGFP which were Black Swiss. Adult male and female animals age >P60 were used in the study. Mice were separated based on sex after weaning at P21 and group-housed (2-4 mice per cage). Animals had ad libitum access to food and water and were on a 12-h light/dark cycle with lights on at 7 AM. Guidelines of the Canadian Council on Animal Care were followed, and all experimental procedures were approved by the Faculty of Medicine Animal Care Committee at the University of Toronto. 42 mice were used for the entire study, with similar numbers of males and females.

Brain slicing and electrophysiology

Slicing and electrophysiology followed procedures described previously (*16*). An intraperitoneal injection of chloral hydrate (400 mg/kg) was given to anesthetize mice prior to decapitation. The brain was rapidly extracted in ice cold sucrose ACSF (254 mM sucrose, 10 mM D-glucose, 26 mM $NaHCO_3$, 2 mM $CaCl_2$, 2 mM $MgSO_4$, 3 mM KCl and 1.25 mM NaH_2PO_4). 400 µm thick

coronal slices of prefrontal cortex (Bregma 2.2 - 1.1) were obtained on a Dosaka linear slicer (SciMedia, Costa Mesa, CA, USA). Slices were left to recover for at least 2 hours in oxygenated (95% O_2, 5% CO_2) ACSF (128 mM NaCl, 10 mM D-glucose, 26 Mm $NaHCO_3$, 2 mM $CaCl_2$, 2 mM $MgSO_4$, 3 Mm KCl, and 1.25 mM NaH_2PO_4) at 30°C before being used for electrophysiology or two-photon calcium imaging. Brain slices were transferred to the stage of a BX51WI microscope (Olympus, Tokyo, Japan) and perfused with oxygenated ACSF at 30°C. Recording electrodes (2 - 4 MΩ) containing patch solution (120 mM potassium gluconate, 5 mM KCl, 10 mM HEPES, 2 mM $MgCl_2$, 4 mM K_2-ATP, 0.4 mM Na_2-GTP and 10 mM sodium phosphocreatine, pH adjusted to 7.3 using KOH) were used to patch pyramidal neurons in layer 6 - 6b based on morphology and proximity to white matter. Only regular spiking neurons were included. Multiclamp 700B amplifier at 20 kHz with Digidata 1440A and pClamp 10.7 software (Molecular devices) were used for data acquisition. All recordings were compensated for liquid junction potential (14 mV). Voltage-clamp responses were examined at -75 mV and in current-clamp at rest or starting from -70 mV.

Optogenetics

5 ms pulses of blue light (473 nm) were delivered through the 60X objective lens with an LED (Thorlabs, 2 mW) to excite channelrhodopsin containing cholinergic fibers. Pattern of stimulation was as in a previous study, with 8 pulses of light delivered in a frequency accommodating manner (*16*).

Pharmacology

Acetylcholine (1mM, Sigma) was used to exogenously stimulate cholinergic receptors. Atropine (200 nM, Sigma) and Dihydro-β-erythroidine (DHBE, 10 μM, Tocris) were used to competitively block muscarinic receptors and β2 subunit-containing nicotinic receptors respectively. Mecamylamine (5 μM, Tocris) was used to further non-competitively block nicotinic receptors. Phospholipase C activator m-3M3FBS (25 μM, Tocris) was used to cleave GPI-anchored Lynx prototoxins and the inactive ortholog o-3M3FBS (25 μM, Tocris) was used as a control (*47*). Cyclodextrin (1 mM, Tocris) was included in a small subset of experiments to improve solubility of 3M3FBS compounds, but no further improvement in efficacy was observed. Water soluble recombinant Ly6g6e (0.5 mg/ml) was obtained by custom purification (Creative Biomart) and used for exogenous application at 1: 1000 and 3:1000 dilution. Effects on nicotinic receptors were not distinguishable between the two different protein concentrations. Only freshly thawed protein aliquots were used for experiments.

Two-photon imaging

Two-photon imaging of GCaMP6s calcium signals in L6 neurons was performed using a 60× water-immersion objective with 0.90 numerical aperture using an Olympus Fluoview FV1000 microscope and a Titanium-Sapphire laser sapphire laser (Newport) at 930nm. Images were sampled at 512 x 512 pixels (2.4 pixels/μm) at a frame rate of 0.9 Hz. Following a 2-minute washout period for this initial application, GCaMP6s calcium signals were measured in response to acetylcholine (1 mM, 15 s). The cellular responses to acetylcholine were measured at baseline, then after application of competitive nicotinic receptor antagonist DHBE (10 μM, 10 min), and again after the addition of muscarinic antagonist atropine (200 nM, 10 min).

Dual color two-photon imaging (910 nm excitation, using 570 nm dichroic mirror with green (540-595 nm) and red (570-620 nm) filters) was performed in brain slices of triple transgenic *Chrna5*-Cre$^{/+}$Ai14$^{/+}$*Syt6*-EGFP$^{/+}$ mice to examine overlap in fluorescent reporter expression between Chrna5+ and Syt6+ neurons. Z-stacks of 30 frames acquired in 1-µm steps were taken in layer 6 of mPFC slices and the maximum projection used to count cells with the cell counter feature in Fiji. A set of mPFC brain slices from *Chrna5*-Cre$^{/+}$Ai14$^{/+}$*Syt6*-EGFP$^{/+}$ mice were also fixed and mounted for confocal imaging with LSM880 (Leica) microscope.

Single cell RNAseq analysis

Single cell RNAseq data for Anterior Cingulate Cortex (ACA) of adult mice was taken from the ACA and MOP Smart-Seq (2018) database, with cell-type annotations from Whole cortex & Hippocampus Smart-Seq (2019) database from the Allen Institute for Brain Science at https://portal.brain-map.org/atlases-and-data/rnaseq (*48*, *49*). Single cell analysis was performed using the R package Seurat (v 4.04). Layer 5 and 6 glutamatergic neurons were selected and sorted into three cell classes based on their expression of *Chrna5* and *Syt6* genes: those expressing only *Chrna5* (Chrna5+, n = 243), only *Syt6* (Syt6+, n = 834), or both *Chrna5* and *Syt6* (Chrna5+Syt6+, n = 564). Expression (copies per million) greater than zero was used as the threshold. 781 cells did not express either *Chrna5* or *Syt6* and were not used in subsequent analyses. Rare cell types with fewer than 10 cells per group are not shown in the heatmap in figure 5 but are included for the differential expression analysis. The FindMarkers function in Seurat was used to identify genes differentially expressed between the Chrna5+ and Chrna5+Syt6+ populations. Adjusted p value < 0.05 was used as the cutoff for identifying differentialy expressed genes.

Analysis and statistics

Analysis of electrophysiological data was conducted on Clampfit 10.7 and Axograph. Rising slope was measured by fitting a line to the first 50ms of the optogenetic cholinergic responses. Cholinergic response magnitude in voltage clamp was determined by peak current (picoamperes) and charge transfer (picocoulombs) measured by the area under the current response for 1 second.

GCaMP6s imaging data were extracted using the multi-measure feature in Fiji. Maximum projections across time for each experiment were first used to identify acetylcholine-responsive cells and add them to the ROI manager, then fluorescence intensity at all timepoints for each cell was measured. Fluorescence was normalized to the background fluorescence averaged over the first 10 frames. Area under the peak (AUP) of the signal after baseline correction was used to quantify the magnitude of cells' response to acetylcholine. Percentage response remaining after DHBE and DHBE+Atropine was calculated from the cell AUP before and after the blockers.

GraphPad Prism 8 was used for statistical analysis and plotting graphs. Bar graphs depicting mean with standard error and boxplots with median and quartiles are shown. Effect sizes are reported as Cohen's d for major results (*50*). Unpaired t-tests or Mann-Whitney tests were used when comparing response properties between cell types, and paired t-test or Wilcoxon test to quantify effect of pharmacological manipulations within cells. Kolmogorov-Smirnov and Fisher's exact tests were used to compare cumulative distributions and proportions of cells respectively.

Results

Chrna5 expression identifies a distinct population of 'acetylcholine super-responder' neurons with stronger and faster-onset optogenetic cholinergic responses

Chrna5 is expressed in deep-layer pyramidal neurons in the prefrontal cortex and thought to modulate their nicotinic receptor properties to improve attentional processing. However, characterization of prefrontal *Chrna5*-expressing (Chrna5+) neurons has not been undertaken previously due to a lack of viable labeling strategies. Using recently available *Chrna5*-Cre mice (*34*), we generated triple transgenic *Chrna5*-Cre$^{/+}$Ai14$^{/+}$ChAT-ChR2$^{/+}$ mice (**Fig 1A**) to interrogate optogenetic cholinergic responses in labeled Chrna5+ neurons. These mice expressed tdTomato in Chrna5+ neurons and channelrhodopsin 2 in cholinergic axons as seen by two-photon imaging (**Fig 1B**). We recorded endogenous responses to optogenetic cholinergic stimulation by patch-clamp electrophysiology in mPFC slices and compared the properties of labeled Chrna5+ and unlabeled Chrna5- pyramidal neurons in layer 6 (**Fig 1C**). Neurons identified by their *Chrna5* expression showed larger-amplitude cholinergic responses with significantly faster onset compared to other unlabeled deep-layer pyramidal neurons (**Fig 1D-F**). The rising slope was significantly larger in Chrna5+ neurons (220 ± 32 pA/s, 24 cells from 4 mice) compared to unlabeled neurons (123 ± 22 pA/s, 15 cells; $t_{(37)} = 2.19$, $P = 0.02$; Cohen's d: 0.72). Similarly, peak current evoked by optogenetic acetylcholine release was greater in Chrna5+ neurons (15 ± 2 pA) compared to unlabeled neurons (8 ± 1 pA, $t_{(37)} = 2.52$, $P = 0.02$; Cohen's d: 0.83), as well as the area of the cholinergic response ($t_{(37)} = 2.06$, $P = 0.046$). Intrinsic electrophysiological properties including resting membrane potential, input resistance, capacitance, spike threshold, amplitude and rheobase did not differ between Chrna5+ and unlabeled neurons (**Supplementary table 1**). As reported previously in a broader layer 6 population (*16*), cholinergic responses in Chrna5+ neurons were under presynaptic muscarinic autoinhibitory control, which was relieved by atropine resulting in even larger responses (94 ± 42% increase). The addition of nicotinic antagonist DHBE eliminated optogenetic cholinergic responses (99 ± 3 % reduction), indicating the predominant contribution of β2 subunit-containing nicotinic receptors in Chrna5+ neurons. Our initial characterization of Chrna5+ neurons revealed them to be acetylcholine 'super-responders' with stronger and faster onset cholinergic responses distinct from other deep-layer pyramidal neurons.This prompted us to question how these cells differ from other well-defined layer 6 neurons labeled by *Syt6* expression (Syt6+).

Syt6 has been extensively used as a marker to characterize layer 6 corticothalamic neurons and their function during PFC-dependent tasks (*28*, *30*, *31*, *51*). Yet, the extent of overlap between *Chrna5* and *Syt6* expressing deep-layer pyramidal neuron populations is unclear. Therefore, we adopted an imaging strategy to visualize the distribution of Chrna5+ and Syt6+ neurons in the PFC and determine the exact proportion of distinctive non-overlapping Chrna5+ neurons. We generated a compound transgenic *Chrna5*-Cre$^{/+}$Ai14$^{/+}$*Syt6*-EGFP$^{/+}$ mouse to simultaneously express tdTomato in Chrna5+ neurons and EGFP in Syt6+ neurons and performed confocal and two photon imaging of the endogenous fluorescence of these reporters in mPFC brain slices. Chrna5+ and Syt6+ neurons were both present primarily in layer 6, with a few Chrna5+ neurons in layer 5 (**Fig 1G, I**). Closer investigation confirmed the existence of a substantial proportion of exclusively

Chrna5+ neurons (37% of all labeled cells) which do not express *Syt6*, in addition to overlapping Chrna5+Syt6+ neurons (39%) which express both markers, and exclusively Syt6+ neurons (24%) which do not express *Chrna5* (N = 4 mice, **Fig 1H, J**). Thus, nearly half of all *Chrna5*-expressing neurons are not labeled by *Syt6*-expression and would be excluded in previous studies using *Syt6*-Cre mice.

Calcium imaging in Chrna5+ and Syt6+ layer 6 populations reveal a distinct subset of Chrna5+ neurons with highly resilient nicotinic receptor-mediated responses.

We next examined population level cholinergic responses in Chrna5+ and Syt6+ neurons to identify properties that distinguish the distinct subset of Chrna5+ neurons not found with Syt6-labeling approaches. We measured acetylcholine-evoked signals in multiple neurons simultaneously using *ex vivo* GCaMP6s calcium imaging in brain slices. We generated transgenic mice expressing GCaMP6s in either Chrna5+ (*Chrna5*-Cre Ai96) or Syt6+ (*Syt6*-Cre Ai96) neurons and performed two-photon imaging of mPFC layer 6 (**Fig 2A**). Calcium signals evoked by acetylcholine (1 mM, 15 s) were measured in Chrna5+ (supplementary video 1) and Syt6+ neurons (supplementary video 2). Changes in the calcium signal and proportions of acetylcholine-responsive neurons were measured after the application of competitive nicotinic receptor antagonist DHBE and addition of muscarinic antagonist atropine (**Fig 2A, B**). The proportion of acetylcholine-evoked calcium signals remaining after the application of the competitive nicotinic antagonist DHBE (10 µM, 10 min) was significantly greater in Chrna5+ neurons (35 ± 3 % of baseline, n = 71 cells, 6 mice; Fig 2C i), compared to Syt6+ neurons (21 ± 3% of baseline, n = 112 cells, 7 mice; Mann Whitney U = 2400, $P < 10^{-4}$). The cumulative distribution of responses remaining after DHBE was significantly right shifted in Chrna5+ neurons compared to Syt6+ neurons (Fig 2C ii, Kolmogorov Smirnov D = 0.37, $P < 10^{-4}$). A majority of Chrna5+ neurons (~83%) still showed acetylcholine-evoked responses after DHBE, whereas only fewer Syt6+ neurons (~50%) retained their responses, with a complete elimination of acetylcholine-evoked responses in the rest (Fig 2C iii, Fisher's exact test: $P < 10^{-4}$). Yet, the addition of muscarinic antagonist atropine did not attenuate the striking differences between Chrna5+ and Syt6+ neurons, raising the possibility of an underlying nicotinic mechanism (**Fig 2D**). In the presence of DHBE+ atropine, a subset of Chrna5+ neurons still showed substantial acetylcholine-evoked calcium signals (6 ± 1 % of baseline; Fig 2Di), whereas almost all Syt6+ neurons' responses were completely blocked (0.2 ± 0.1 % of baseline; Mann Whitney U = 2083, $P < 10^{-4}$) as seen from the cumulative distribution (Fig 2D ii, Kolmogorov Smirnov D = 0.36, $P < 10^{-4}$). The proportion of Chrna5+ and Syt6+ neurons showing acetylcholine-evoked responses after DHBE+ Atropine was significantly different (41% vs 6%, Fisher's exact test: $P < 10^{-4}$, **Fig 2D iii**).

While optogenetic cholinergic responses in Chrna5+ neurons were eliminated by the combination of DHBE and atropine, residual responses to strong stimulation with exogenous acetylcholine were observed in a large Chrna5+ subset following DHBE and atropine. Since DHBE is a competitive antagonist, it can be outcompeted by exogenous acetylcholine at high affinity nicotinic receptors. We hypothesized that the resilience of exogenous acetylcholine-evoked responses to competitive nicotinic receptor block in a large subset of Chrna5+ neurons indicated high affinity nicotinic receptors which would require non-competitive blockers to be completely blocked. We switched

to patch-clamp electrophysiology to test this hypothesis and investigate acetylcholine-evoked spiking in individual Chrna5+ and Syt6+ neurons. We recorded current clamp responses to acetylcholine (1 mM, 15 s) in labeled Chrna5+ and Syt6+ neurons from *Chrna5*-Cre$^{/+}$Ai14$^{/+}$ and *Syt6*-Cre$^{/+}$Ai14$^{/+}$ or *Syt6*-EGFP mice respectively (**Fig 2E**). Chrna5+ neurons showed stronger acetylcholine-evoked firing: attaining significantly higher peak firing frequency (29 ± 6 Hz, n=12 cells, 6 mice; $t_{(24)} = 2.74$, $P = 0.01$; Cohen's d: 1.08) compared to Syt6+ neurons (13 ± 2 Hz, n = 14 cells, 5 mice; Fig 3B). The intrinsic electrophysiological properties of Chrna5+ and Syt6+ neurons did not show statistically significant differences (**Supplementary table 2**). We next examined the sensitivity of acetylcholine-evoked firing to competitive nicotinic receptor block by DHBE in the presence of atropine. Acetylcholine-evoked firing was completely eliminated in all Syt6+ neurons (**Fig 2F**) whereas a large subset of Chrna5+ neurons (7/11) retained their ability to respond to acetylcholine (Average peak firing rate: 6 ± 2 Hz; $t_{(19)} = 3.22$, $P = 0.004$, unpaired t-test) demonstrating similar resilience to competitive nicotinic receptor block as observed with calcium imaging. We used the non-competitive nicotinic receptor blocker mecamylamine (*54*, *55*) to test our hypothesis that nicotinic receptors in this Chrna5+ subset were higher affinity and therefore allowed exogenous acetylcholine to outcompete DHBE. The addition of 5 μM mecamylamine was sufficient to eliminate acetylcholine-evoked firing in all the Chrna5+ neurons that were resilient to competitive nicotinic block ($t_{(4)} = 5.14$, $P = 0.007$, paired t-test; Fig 2F). Together, our calcium imaging and electrophysiology experiments neurons revealed the existence of a distinct subset of Chrna5+ neurons that were dissimilar to Syt6+ neurons, with high affinity nicotinic responses that were resilient to competitive nicotinic antagonism. To answer why enhanced cholinergic responses are found only in the Chrna5+ subset that is distinct from Syt6+ neurons, we turned to single-cell RNAseq to understand the diversity of Chrna5+ neurons and the molecular determinants of their cholinergic properties.

Single-cell transcriptomics identifies Chrna5+ subplate neurons with distinct expression pattern of Lynx genes modulating cholinergic function

We sought to identify whether the exclusive Chrna5+ neurons arise from a different set of cell populations than Syt6+ neurons. Therefore, we extracted gene expression data of L5-6 glutamatergic neurons (n = 2422 cells) in the mouse anterior cingulate cortex from the Allen Institute single cell RNAseq databases (*48*, *49*, *56*). We classified these deep-layer pyramidal neurons into 3 groups as seen with imaging: those expressing only *Chrna5* (Chrna5+, n= 243), both *Chrna5* and *Syt6* (Chrna5+ Syt6+, n = 834), or only *Syt6* (Syt6+, n = 564) **(Fig 3A)**. 781 cells showed no expression of *Chrna5* or *Syt6* and consisted primarily of L6 Intratelencephalic cells which have been previously shown to have purely muscarinic M2/M4 mediated hyperpolarizing cholinergic responses (*16*, *57*). We focused on the Chrna5+, Syt6+ and Chrna5+Syt6+ groups to examine their transcriptomic differences. Single-cell analysis revealed that the Chrna5+ group primarily included L6b (44%), L5 near-projecting (L5NP, 19%), and L6CT neurons (30%), whereas the Chrna5+Syt6+ and Syt6+ groups were predominantly composed of L6CT neurons (>90%) **(Fig 3B)**. We examined the expression of marker genes in these respective groups to validate our cell-classification. To our surprise, Chrna5+ neurons showed distinctive expression of several marker genes- *Ctgf, Cplx3, Kcnab1, Lpar1* **(Fig 3B,C)** associated with subplate neurons (*35*, *58*). Subplate neurons are vital for early brain development and L6b neurons are considered

descendants of this early-born population (*36*, *37*, *59*). Notably, the highest fold enrichment among all differentially expressed genes in Chrna5+ neurons was found for subplate markers *Ctgf* (Fold change, 5.69) and *Cplx3* (3.81) (**Table 1)**. Overall, Chrna5+ neurons including both L5NP and L6b subpopulations highly express subplate marker genes. In contrast, *Syt6*-expressing Chrna5+Syt6+ and Syt6+ groups are only enriched in the corticothalamic markers *Foxp2* and *Syt6*, consistent with their corticothalamic subtype. These results support our imaging, electrophysiological, and pharmacological results suggesting the exclusive Chrna5+ population is distinct from typical L6CT *Syt6*-expressing neurons.

Next, we examined differential expression of genes with known effects on postsynaptic cholinergic responses to identify molecular changes predictive of Chrna5+ 'super-responders' with high-affinity nicotinic responses (**Fig 3D-E**). We selected cholinergic receptor genes (nicotinic *Chrna5-2, Chrna7, Chrnb2-4,* and muscarinic subunits *Chrm1-4*), acetylcholinesterase (*Ache*), and members of the family of genes that encode lynx proteins (*Ly6e, Ly6h, Ly6g6e, Lynx1, Lypd1, Lypd6, Lypd6b*) known to allosterically modulate nicotinic receptor responses (*38*). We found substantial and highly significant changes primarily in the expression of three lynx prototoxins *Lypd1*, *Ly6g6e* and *Lypd6b* **(Fig 3D)**. While both Chrna5+ and Chrna5+Syt6+ populations express *Chrna5,* there was slightly higher expression of *Chrna5* (25% increase) as well as lower expression of the inhibitory muscarinic receptor *Chrm2* (20% decrease) in Chrna5+Syt6+ neurons. There were no significant differences in other nicotinic and muscarinic subunit expression between the two groups. Acetylcholinesterase, the enzyme that breaks down acetylcholine was highly expressed (50% increase) in Chrna5+ neurons, which may benefit their nicotinic responses by protecting receptors from overactivation and desensitization. The fold-change of the genes in figure 3E between Chrna5+ and Chrna5+Syt6+ neurons is shown in **Supplementary table 3**.

Notably, the top three genes with highest fold change in Chrna5+ neurons were the GPI-anchored lynx prototoxins: Lynx2 encoded by *Lypd1* (Fold change: 2.55), *Ly6g6e* (2.03), and *Lypd6b* (1.51). Ly6g6e is thought to potentiate nicotinic receptors and slows nicotinic receptor desensitization (*39*) which might contribute to high-affinity nicotinic responses in Chrna5+ neurons. Lypd6b has unknown effects (*60*) while Lynx2 is thought to inhibit α4β2 nicotinic receptors (*61*). Lynx2 may also intracellularly suppress expression of lower affinity α4β2 receptors (*39*) indirectly promoting the preferential expression of α5 containing high affinity nicotinic receptors in Chrna5+ neurons. However, other lynxes such as Lynx1 which negatively modulates α4β2 receptors (*41*) were expressed at similar levels in the majority of cells across all three groups. The distinct pattern of expression of specific lynxes in Chrna5+ neurons suggests unexpectedly complex endogenous control of nicotinic responses in these prefrontal subplate neurons.

Cell type specific modulation of optogenetic nicotinic responses by endogenous GPI-anchored lynxes

Our transcriptomic analyses suggest that cells capable of fast and strong responses to optogenetic release of endogenous acetylcholine contain complex molecular machinery to regulate these responses. It is possible that this regulation endows deep layer prefrontal neurons with greater dynamic range in responding to acetylcholine. To examine whether this transcriptomic prediction is accurate, we sought to experimentally perturb endogenous lynx modulation. Members of the

lynx-family are GPI-anchored (**Fig 4A**), and work in cell expression systems (*39*) suggests these anchors can be cleaved via activation of phospholipase C (PLC). The potential impact of such GPI cleavage on nicotinic responses in a native system is not well understood. Perturbing lynx-mediated control could affect endogenous nicotinic properties in a complex manner (**Fig 4A**) since both positive (eg. Ly6g6e) and negative modulatory lynxes (eg. Lynx1) are expressed. To cleave GPI-anchored proteins, we used the PLC activator compound m-3M3FBS (*47*, *62–64*). Nicotinic responses of deep layer pyramidal neurons from ChAT-ChR2 mice to optogenetic acetylcholine release were recorded in the continuous presence of atropine before and after treatment with m-3M3FBS (25µM, 5 min; **Fig 4B**). The rising slope of the nicotinic responses showed a significant increase after m-3M3FBS treatment (23 ± 17%; Paired Cohen's d = 0.83; $P = 0.008$, Wilcoxon matched-pairs test), compared to the baseline change observed in the same cells prior to PLC activation (-6 ± 4%; 8 cells, 6 mice; **Fig 4C**). This increase was not observed with the inactive ortholog o-3M3FBS that does not activate PLC (Paired Cohen's d = 0.09, $P = 0.625$, Wilcoxon matched-pairs test, data not shown). The area under the nicotinic response known as charge transfer also showed a statistically significant increase following PLC activation (22 ± 7%; Cohen's d = 1.68; $P = 0.016$, Wilcoxon matched-pairs test; **Fig 4D**), compared to baseline change (-9 ± 6%). Thus, PLC activation causes a specific increase in nicotinic receptor responses, presumably due to cleavage of inhibitory GPI-anchored lynxes such as Lynx1. This result confirmed endogenous lynx modulation of optogenetic cholinergic responses in intact brain slices and validated our transcriptomic prediction of strong endogenous lynx regulation of nicotinic receptors in deep layer neurons.

Our transcriptomics results (Fig 3D) predicted that cell-type specific differences in Lynx modulation with enhanced expression of *Lypd1*, *Ly6g6e* and *Lypd6b* prototoxins in Chrna5+ neurons lead to the different cholinergic properties of *Chrna5* versus *Syt6*-expressing neurons. To validate this prediction experimentally, we tested whether exogenous application of a specific lynx prototoxin exerts differential effects in *Chrna5* and *Syt6*-expressing neurons. Prior work suggests the direction of these effects may be difficult to predict, however, since soluble and endogenous GPI-anchored prototoxins have different effects on nicotinic receptors (*41*). Since previous work predicts a substantial modulatory role for endogenous Ly6g6e, we obtained purified water-soluble recombinant Ly6g6e protein and examined its effects on optogenetic nicotinic responses in labeled Chrna5+ and Syt6+ neurons (**Fig 4F**). These experiments were conducted in *Chrna5*-Cre$^{/+}$Ai14$^{/+}$ChAT-ChR2$^{/+}$ and *Syt6*-Cre$^{/+}$Ai14$^{/+}$ChAT-ChR2$^{/+}$ mice. We hypothesized that the modulation of Chrna5+ neuronal nicotinic receptors by endogenous Ly6g6e would occlude the effect of exogenous soluble Ly6g6e, whereas Syt6+ neurons would be altered by exposure to the exogenous Ly6g6e (Fig 4G). Consistently, we found that 10 minute application of soluble Ly6g6e did not significantly alter the amplitude of optogenetically evoked nicotinic responses in labeled Chrna5+ neurons (Change in peak = -2.1 ± 1.2 pA, $t_{(6)} = 1.79$, $P = 0.12$, paired t-test). However, in labeled Syt6+ neurons lacking endogenous expression of *Ly6g6e*, exogenous application of soluble Ly6g6e caused a significant decrease in the amplitude (Change in peak = -10 ± 1.8 pA, $t_{(8)} = 5.60$, $P < 0.001$, paired t-test; **Fig 4H**). The change in peak and area of the nicotinic responses caused by solube Ly6g6e was significantly different between Chrna5+ and Syt6+ neurons (change in peak : $t_{(14)} = 3.43$, $P = 0.004$; Change in area: $t_{(14)} = 2.53$, $P = 0.024$, Unpaired t test; **Fig 4I - J**).

Our work examines the effects of GPI-anchored lynx prototoxins on native nicotinic receptor-mediated optogenetic responses, advancing from work in heterologous expression systems. These results are a first step in showing how endogenous lynx regulation of nicotinic

responses can act in a complex cell-type specific fashion leading to specialized cholinergic properties in a subset of neurons. Overall, our study reveals a previously uncharacterized population of *Chrna5*-expressing subplate neurons in the prefrontal cortex that are exquisitely sensitive to acetylcholine, with differential expression of several lynx prototoxin genes that allow flexible tuning of their high-affinity nicotinic responses (**Fig 5**).

Discussion (1106 words)

With optophysiological approaches in *Chrna5*-Cre transgenic mice, we identified a subpopulation of prefrontal *Chrna5*-expressing neurons with faster and stronger cholinergic activation and high-affinity nicotinic responses. Transcriptomic analysis revealed these Chrna5+ cholinergic 'super-responders' to express markers associated with subplate neurons, a developmentally-defined population associated with cortical layer 6b in adult rodents. These neurons show specific expression pattern of several GPI-anchored lynx prototoxins known to modulate nicotinic receptor function. Finally, by experimentally perturbing endogenous GPI-anchored lynx and exogenous application of a cell-type specific lynx, we revealed complex lynx-mediated control of endogenous nicotinic receptor function in prefrontal deep-layer neurons.

Specialized cholinergic properties of Chrna5-expressing neurons

The functional impact of the auxiliary alpha5 nicotinic subunit in its native neuronal environment is unclear. Previous work extrapolated the neurophysiological contributions of alpha5 to high-affinity nicotinic receptors based on results of cell system experiments and work in rodents deleted for *Chrna5* (*13*, *16*, *22*, *65*, *66*). Here, *Chrna5*-Cre mice allowed us to affirmatively demonstrate that neurons expressing the alpha5 nicotinic subunit respond faster and more strongly to endogenous acetylcholine. This cholinergic heterogeneity among layer 6 neurons prompted a larger scale comparison between Chrna5+ neurons and a well-defined layer 6 population labeled by *Syt6* (*29*). These experiments revealed a subset of Chrna5+ cholinergic 'super-responders' with high affinity nicotinic responses that were not found in Syt6+ neurons.

Heterogeneity of cell types expressing Chrna5

Previously, the deep-layer cell types expressing *Chrna5* were uncharacterized, and generally thought to include L6CT neurons (*8*). Investigation of L6CT neurons have relied on *Syt6*-Cre and *Ntsr1*-Cre mouse lines that label similar sets of neurons (*27–29*), with only *Syt6*-Cre mice successfully labeling this population in prefrontal cortex (*31*). L6CT neurons act to control attention through their thalamic projections (*67*, *68*), as well as their intracortical excitatory and inhibitory outputs (*69–71*). L6CT neurons labeled by *Syt6* or *Ntsr1* expression are excited by acetylcholine (*32*, *72*), but it was unclear what proportion of these cells were modulated by the α5 nicotinic subunit and the degree to which their nicotinic response relied on *Chrna5* expression. Strikingly, our experiments reveal that the cholinergic super-responders with high affinity nicotinic receptors appear to be from the population of *Chrna5*-labeled neurons that lack *Syt6*-labeling. Our transcriptomic analysis demonstrates that majority of this likely population of Chrna5+ 'super-responders' arise from L5 Near-Projecting and L6b neurons, populations that express multiple markers that link them to the developmental subplate. These enigmatic cells are remnants of the earliest-born cortical neurons that serve as a relay for establishing connections between cortex and thalamus (*73*, *74*). Cholinergic innervation begins early in development and

subplate neurons already receive cholinergic inputs at birth (*75*), highlighting their role in developmental cholinergic modulation.

Chrna5- a marker for subplate cells

In contrast to L6CT neurons, subplate neurons are relatively uncharacterized due to the lack of transgenic mice that definitively label all subtypes as well as the inaccessibility of the available lines for *in vivo* targeting. We found Chrna5+ cholinergic super-responders predominantly arise from neurons that are not labeled by Syt6. Transcriptomic analysis (Fig 5, Table 1) suggests that this Chrna5+ population is enriched for known subplate markers *Ctgf* (Connective tissue growth factor), *Cplx3* (Complexin 3), *Kcnab1,*and *Lpar1* (*35*, *76*, *77*). Significantly, the lynx prototoxin and nicotinic receptor modulator *Ly6g6e*, which is highly expressed in Chrna5+ neurons, is also a marker of subplate neurons (*78*). Our study is the first to identify enhanced cholinergic activation regulated by *Chrna5* and lynx-gene expression in subplate/L6b neurons. Subplate neurons have recently been found to strongly regulate cortical output through their intracortical connections (*79*, *80*). Enhanced cholinergic activation in these neurons will have different consequences for prefrontal processing, challenging the popular conception that cholinergic modulation of attention occurs only through top-down control of thalamic input by L6CT neurons.

Molecular determinants of nicotinic receptor properties in Chrna5+ neurons

Our transcriptomic analysis revealed enhanced expression of GPI-anchored lynx prototoxin genes *Ly6g6e*, *Lypd1*, and *Lypd6b* in Chrna5+ neurons (Fig 5). Lynx proteins are well known modulators of nicotinic receptor properties and trafficking (*41*, *43*), but most of the insight into their actions comes from heterologous cell systems, deletion, and overexpression experiments. Relatively little is known about their effects on nicotinic receptors in their native environment. In expression systems, Ly6g6e potentiates α4β2 nicotinic responses and slows their desensitization (*39*), predicting cholinergic responses in Chrna5+ neurons would be resistant to desensitization, as has been implied by *Chrna5* deletion work (*16*). On the other hand, Lynx2 is a negative nicotinic modulator that increases desensitization of α4β2 nicotinic receptors (*61*), and is selectively expressed in the medial PFC (*81*). While Lynx2 is thought to act intracellularly to reduce surface expression of α4β2 nicotinic receptors (*39*), it may act selectively on the $(\alpha4)_3(\beta2)_2$ receptor subtype which are lower affinity (*65*, *82*) and indirectly promote expression of high affinity α5-containing $(\alpha4)_2(\beta2)_2\alpha5$ nicotinic receptors. The effect of Lypd6b on $(\alpha4)_2(\beta2)_2\alpha5$ nicotinic receptors found in Chrna5+ neurons is yet to be determined and may further contribute to the complex control of their nicotinic responses (*60*). In addition, Lynx1, a well known negative modulator of α4β2 nicotinic receptors (*42*, *83–85*) is also expressed uniformly across all Chrna5+ and Syt6+ neurons. Consistent with such complex regulation by lynxes, our experiments confirmed that removing GPI-anchored lynxes increases nicotinic response onset speed and amplitude in layer 6 neurons, potentially due to removal of Lynx1. In contrast, exogenous application of recombinant Ly6g6e protein had different effects in *Chrna5* and *Syt6*-expressing neurons, consistent with the differential lynx modulation in Chrna5+ neurons predicted by transcriptomics.

Functional consequences

The effects of lynxes on nicotinic receptor function have so far been determined by heterologous expression systems (*39*, *61*), knockout studies (*61*, *81*), exogenous application of recombinant water-soluble lynx proteins (*86*, *87*), and more recently viral overexpression in the brain (*42*, *88*). Our results are highlight complex endogenous regulation of optogenetic nicotinic responses by multiple GPI-anchored lynxes. Expression of inhibitory lynxes and high levels of acetylcholinesterase in Chrna5+ neurons suggest that their responses are restrained and our experiments likely underestimated their nicotinic receptor function. These responses could be dramatically enhanced when acetylcholinesterase and inhibitory lynx modulation is reduced through other signaling mechanisms. Such flexible tuning of nicotinic responses by lynx prototoxins in Chrna5+ neurons can provide greater dynamic range and poises them to be key players during attentional processing (Fig 9). A recent study found that developmental increase in Lynx1 expression in corticocortical neurons suppressed their nicotinic responses and preventing this by viral knockdown of Lynx1 led to altered cortical connectivity and impaired attention (*42*). Thus cell-type specific changes in lynx expression during development are critical for maturation of attention circuits. It is of interest to examine such changes during development in Chrna5+ neurons and how they differ from Syt6+ neurons.

Our study reveals a distinct group of 'acetylcholine super-responder' neurons in the prefrontal cortex identified by *Chrna5*-expression that include subplate neurons vital for cortical development. We identify that their high affinity α5 subunit-containing nicotinic receptors are under complex regulation by several lynx prototoxins and acetylcholinesterase. *Chrna5*-Cre mice are a valuable tool for future studies examining the in vivo role of these specialized neurons.

References

1. J. W. Dalley, R. N. Cardinal, T. W. Robbins, Prefrontal executive and cognitive functions in rodents: neural and neurochemical substrates. *Neuroscience & Biobehavioral Reviews*. **28**, 771–784 (2004).

2. J. McGaughy, J. W. Dalley, C. H. Morrison, B. J. Everitt, T. W. Robbins, TW. Robbins, Selective behavioral and neurochemical effects of cholinergic lesions produced by intrabasalis infusions of 192 IgG-saporin on attentional performance in a five-choice serial reaction time task. *J Neurosci*. **22**, 1905–13 (2002).

3. J. W. Dalley, D. E. Theobald, P. Bouger, Y. Chudasama, R. N. Cardinal, T. W. Robbins, Cortical Cholinergic Function and Deficits in Visual Attentional Performance in Rats Following 192 IgG-Saporin-induced Lesions of the Medial Prefrontal Cortex. *Cerebral Cortex*. **14**, 922–932 (2004).

4. H. J. Gritton, W. M. Howe, C. S. Mallory, V. L. Hetrick, J. D. Berke, M. Sarter, Cortical cholinergic signaling controls the detection of cues. *Proc Natl Acad Sci U S A*. **113**, E1089-97 (2016).

5. F. Briggs, W. M. Usrey, Emerging views of corticothalamic function. *Current Opinion in Neurobiology*. **18** (2008), pp. 403–407.

6. J. Voigts, C. A. Deister, C. I. Moore, Layer 6 ensembles can selectively regulate the behavioral impact and layer-specific representation of sensory deviants. *Elife*. **9** (2020), doi:10.7554/eLife.48957.

7. T. Spellman, M. Svei, J. Kaminsky, G. Manzano-Nieves, C. Liston, Prefrontal deep projection neurons enable cognitive flexibility via persistent feedback monitoring. *Cell*. **184**, 2750-2766.e17 (2021).

8. S. M. Kassam, P. M. Herman, N. M. Goodfellow, N. C. Alves, E. K. Lambe, Developmental excitation of corticothalamic neurons by nicotinic acetylcholine receptors. *J Neurosci*. **28**, 8756–64 (2008).

9. D. W. Sparks, M. K. Tian, D. Sargin, S. Venkatesan, K. Intson, E. K. Lambe, Opposing cholinergic and serotonergic modulation of layer 6 in prefrontal cortex. *Frontiers in Neural Circuits*. **11** (2018), doi:10.3389/fncir.2017.00107.

10. S. Venkatesan, H.-S. Jeoung, T. Chen, S. K. Power, Y. Liu, E. K. Lambe, in *Behavioral Pharmacology of the Cholinergic System* (Springer, Berlin, Heidelberg, 2020), pp. 47–69.

11. U. H. Winzer-Serhan, F. M. Leslie, Expression of alpha5 nicotinic acetylcholine receptor subunit mRNA during hippocampal and cortical development. *The Journal of Comparative Neurology*. **481**, 19–30 (2005).

12. E. Wada, D. McKinnon, S. Heinemann, J. Patrick, L. W. Swanson, The distribution of mRNA encoded by a new member of the neuronal nicotinic acetylcholine receptor gene family (α5) in the rat central nervous system. *Brain Research*. **526**, 45–53 (1990).

13. C. D. C. Bailey, M. De Biasi, P. J. Fletcher, E. K. Lambe, The nicotinic acetylcholine receptor alpha5 subunit plays a key role in attention circuitry and accuracy. *J Neurosci*. **30**, 9241–52 (2010).

14. M. K. Tian, C. D. C. Bailey, M. De Biasi, M. R. Picciotto, E. K. Lambe, Plasticity of prefrontal attention circuitry: upregulated muscarinic excitability in response to decreased nicotinic signaling following deletion of α5 or β2 subunits. *J Neurosci*. **31**, 16458–63 (2011).

15. W. M. Howe, J. L. Brooks, P. L. Tierney, J. Pang, A. Rossi, D. Young, K. Dlugolenski, E. Guillmette, M. Roy, K. Hales, R. Kozak, α5 nAChR modulation of the prefrontal cortex makes attention resilient. *Brain Structure and Function*. **223**, 1035–1047 (2018).

16. S. Venkatesan, E. K. Lambe, Chrna5 is essential for a rapid and protected response to optogenetic release of endogenous acetylcholine in prefrontal cortex. *The Journal of Neuroscience*. **40**, 7255–7268 (2020).

17. W. Han, T. Zhang, T. Ni, L. Zhu, D. Liu, G. Chen, H. Lin, T. Chen, F. Guan, Relationship of common variants in CHRNA5 with early-onset schizophrenia and executive function. *Schizophrenia Research*. **206**, 407–412 (2019).

18. L. J. Bierut, J. A. Stitzel, J. C. Wang, A. L. Hinrichs, R. A. Grucza, X. Xuei, N. L. Saccone, S. F. Saccone, S. Bertelsen, L. Fox, W. J. Horton, S. D. Morgan, N. Breslau, J. Budde, C. R. Cloninger, D. M. Dick, T. Foroud, D. Hatsukami, V. Hesselbrock, E. O. Johnson, J. Kramer, S. Kuperman, P. A. F. Madden, K. Mayo, J. Nurnberger, Jr., O. Pomerleau, B. Porjesz, O. Reyes, M. Schuckit, G. Swan, J. A. Tischfield, H. J. Edenberg, J. P. Rice, A. M. Goate, Variants in the Nicotinic Receptors Alter the Risk for Nicotine Dependence. *Am J Psychiatry*. **165**, 1163 (2008).

19. J. B. Schuch, E. R. Polina, D. L. Rovaris, D. B. Kappel, N. R. Mota, R. B. Cupertino, K. L. Silva, P. O. Guimarães-da-Silva, R. G. Karam, C. A. I. Salgado, M. J. White, L. A. Rohde, E. H. Grevet, C. H. D. Bau, Pleiotropic effects of Chr15q25 nicotinic gene cluster and the relationship between smoking, cognition and ADHD. *Journal of Psychiatric Research*. **80**, 73–78 (2016).

20. U. Maskos, The nicotinic receptor alpha5 coding polymorphism rs16969968 as a major target in disease: Functional dissection and remaining challenges. *Journal of Neurochemistry*. **154**, 241–250 (2020).

21. P. Scholze, S. Huck, The α5 Nicotinic Acetylcholine Receptor Subunit Differentially Modulates α4β2* and α3β4* Receptors. *Frontiers in Synaptic Neuroscience*. **12** (2020), p. 607959.

22. M. S. Prevost, H. Bouchenaki, N. Barilone, M. Gielen, P. J. Corringer, Concatemers to re-investigate the role of α5 in α4β2 nicotinic receptors. *Cellular and Molecular Life Sciences 2020 78:3*. **78**, 1051–1064 (2020).

23. A. M. Thomson, Neocortical layer 6, a review. *Front Neuroanat*. **4**, 13 (2010).

24. F. Briggs, Organizing principles of cortical layer 6. *Front Neural Circuits*. **4**, 3 (2010).

25. S. A. Sorensen, A. Bernard, V. Menon, J. J. Royall, K. J. Glattfelder, T. Desta, K. Hirokawa, M. Mortrud, J. A. Miller, H. Zeng, J. G. Hohmann, A. R. Jones, E. S. Lein, Correlated Gene Expression and Target Specificity Demonstrate Excitatory Projection Neuron Diversity. *Cerebral Cortex*. **25**, 433–449 (2015).

26. C. J. Heath, S. L. King, C. Gotti, M. J. Marks, M. R. Picciotto, Cortico-Thalamic Connectivity is Vulnerable to Nicotine Exposure During Early Postnatal Development through α4/β2/α5 Nicotinic Acetylcholine Receptors. *Neuropsychopharmacology*. **35**, 2324–2338 (2010).

27. J. A. Harris, K. E. Hirokawa, S. A. Sorensen, H. Gu, M. Mills, L. L. Ng, P. Bohn, M. Mortrud, B. Ouellette, J. Kidney, K. A. Smith, C. Dang, S. Sunkin, A. Bernard, S. W. Oh, L. Madisen, H. Zeng, Anatomical characterization of Cre driver mice for neural circuit mapping and manipulation. *Frontiers in Neural Circuits*. **8**, 76 (2014).

28. J. A. Harris, S. Mihalas, K. E. Hirokawa, J. D. Whitesell, H. Choi, A. Bernard, P. Bohn, S. Caldejon, L. Casal, A. Cho, A. Feiner, D. Feng, N. Gaudreault, C. R. Gerfen, N. Graddis, P. A. Groblewski, A. M. Henry, A. Ho, R. Howard, J. E. Knox, L. Kuan, X. Kuang, J. Lecoq, P. Lesnar, Y. Li, J. Luviano, S. McConoughey, M. T. Mortrud, M. Naeemi, L. Ng, S. W. Oh, B. Ouellette, E. Shen, S. A. Sorensen, W. Wakeman, Q. Wang, Y. Wang, A. Williford, J. W. Phillips, A. R. Jones, C. Koch, H. Zeng, Hierarchical organization of cortical and thalamic connectivity. *Nature*. **575**, 195–202 (2019).

29. A. R. Nectow, M. V. Moya, M. I. Ekstrand, A. Mousa, K. L. McGuire, C. E. Sferrazza, B. C. Field, G. S. Rabinowitz, K. Sawicka, Y. Liang, J. M. Friedman, N. Heintz, E. F. Schmidt, Rapid Molecular Profiling of Defined Cell Types Using Viral TRAP. *Cell Reports*. **19**, 655–667 (2017).

30. H. Nakayama, I. Ibañez-Tallon, N. Heintz, Cell-type-specific contributions of medial prefrontal neurons to flexible behaviors. *Journal of Neuroscience*. **38**, 4490–4504 (2018).

31. L. O. Vaasjo, X. Han, A. N. Thurmon, A. S. Tiemroth, H. Berndt, M. Korn, A. Figueroa, R. Reyes, P. A. Feliciano-Ramos, M. J. Galazo, Characterization and manipulation of Corticothalamic neurons in associative cortices using Syt6-Cre transgenic mice. *Journal of Comparative Neurology* (2021), doi:10.1002/CNE.25256.

32. M. K. Tian, C. D. C. Bailey, E. K. Lambe, Cholinergic excitation in mouse primary vs. associative cortex: region-specific magnitude and receptor balance. *Eur J Neurosci*. **40**, 2608–18 (2014).

33. J. L. Ables, A. Görlich, B. Antolin-Fontes, C. Wang, S. M. Lipford, M. H. Riad, J. Ren, F. Hu, M. Luo, P. J. Kenny, N. Heintz, I. Ibañez-Tallon, Retrograde inhibition by a specific subset of interpeduncular α5 nicotinic neurons regulates nicotine preference. *Proc Natl Acad Sci U S A*. **114**, 13012–13017 (2017).

34. G. Morton, N. Nasirova, D. W. Sparks, M. Brodsky, S. Sivakumaran, E. K. Lambe, E. E. Turner, Chrna5-expressing neurons in the interpeduncular nucleus mediate aversion primed by prior stimulation or nicotine exposure. *J Neurosci*, 0023–18 (2018).

35. A. Hoerder-Suabedissen, Z. Molnár, Molecular Diversity of Early-Born Subplate Neurons. *Cerebral Cortex*. **23**, 1473–1483 (2013).

36. H. J. Luhmann, S. Kirischuk, W. Kilb, The superior function of the subplate in early neocortical development. *Frontiers in Neuroanatomy*. **12**, 97 (2018).

37. P. O. Kanold, H. J. Luhmann, The Subplate and Early Cortical Circuits. *http://dx.doi.org/10.1146/annurev-neuro-060909-153244*. **33**, 23–48 (2010).

38. J. M. Miwa, K. R. Anderson, K. M. Hoffman, Lynx Prototoxins: Roles of Endogenous Mammalian Neurotoxin-Like Proteins in Modulating Nicotinic Acetylcholine Receptor Function to Influence Complex Biological Processes. *Frontiers in Pharmacology*. **10**, 343 (2019).

650 39. M. Wu, C. A. Puddifoot, P. Taylor, W. J. Joiner, Mechanisms of inhibition and potentiation of
651 α4β2 nicotinic acetylcholine receptors by members of the Ly6 protein family. *J Biol Chem*. **290**,
652 24509–18 (2015).

653 40. M. P. Demars, H. Morishita, Cortical parvalbumin and somatostatin GABA neurons express
654 distinct endogenous modulators of nicotinic acetylcholine receptors. *Molecular Brain*. **7**, 75
655 (2014).

656 41. J. M. Miwa, Lynx1 prototoxins: critical accessory proteins of neuronal nicotinic acetylcholine
657 receptors. *Current Opinion in Pharmacology*. **56**, 46–51 (2021).

658 42. E. N. Falk, K. J. Norman, Y. Garkun, M. P. Demars, S. Im, G. Taccheri, J. Short, K. Caro, S. E.
659 Mccraney, C. Cho, M. R. Smith, H.-M. Lin, H. Koike, J. Bateh, P. Maccario, L. Waltrip, M. Janis,
660 H. Morishita, Nicotinic regulation of local and long-range input balance drives top-down
661 attentional circuit maturation. *Sci. Adv.* **7** (2021).

662 43. K. R. Anderson, K. M. Hoffman, J. M. Miwa, Modulation of cholinergic activity through lynx
663 prototoxins: Implications for cognition and anxiety regulation. *Neuropharmacology*. **174** (2020),
664 p. 108071.

665 44. S. Gong, M. Doughty, C. R. Harbaugh, A. Cummins, M. E. Hatten, N. Heintz, C. R. Gerfen,
666 Targeting Cre recombinase to specific neuron populations with bacterial artificial chromosome
667 constructs. *Journal of Neuroscience*. **27** (2007), pp. 9817–9823.

668 45. S. Gong, C. Zheng, M. L. Doughty, K. Losos, N. Didkovsky, U. B. Schambra, N. J. Nowak, A.
669 Joyner, G. Leblanc, M. E. Hatten, N. Heintz, A gene expression atlas of the central nervous system
670 based on bacterial artificial chromosomes. *Nature*. **425**, 917–925 (2003).

671 46. L. Madisen, T. A. Zwingman, S. M. Sunkin, S. Wook Oh, H. A. Zariwala, H. Gu, L. L. Ng, R. D.
672 Palmiter, M. J. Hawrylycz, A. R. Jones, E. S. Lein, H. Zeng, A robust and high-throughput Cre
673 reporting and characterization system for the whole mouse brain (2010), doi:10.1038/nn.2467.

674 47. Y. S. Bae, T. G. Lee, J. C. Park, J. H. Hur, Y. Kim, K. Heo, J. Y. Kwak, P. G. Suh, S. H. Ryu,
675 Identification of a Compound That Directly Stimulates Phospholipase C Activity. *Molecular*
676 *Pharmacology*. **63**, 1043–1050 (2003).

677 48. B. Tasic, Z. Yao, L. T. Graybuck, K. A. Smith, T. N. Nguyen, D. Bertagnolli, J. Goldy, E. Garren,
678 M. N. Economo, S. Viswanathan, O. Penn, T. Bakken, V. Menon, J. Miller, O. Fong, K. E.
679 Hirokawa, K. Lathia, C. Rimorin, M. Tieu, R. Larsen, T. Casper, E. Barkan, M. Kroll, S. Parry, N.
680 V. Shapovalova, D. Hirschstein, J. Pendergraft, H. A. Sullivan, T. K. Kim, A. Szafer, N. Dee, P.
681 Groblewski, I. Wickersham, A. Cetin, J. A. Harris, B. P. Levi, S. M. Sunkin, L. Madisen, T. L.
682 Daigle, L. Looger, A. Bernard, J. Phillips, E. Lein, M. Hawrylycz, K. Svoboda, A. R. Jones, C.
683 Koch, H. Zeng, Shared and distinct transcriptomic cell types across neocortical areas. *Nature*. **563**,
684 72–78 (2018).

685 49. Z. Yao, C. T. J. van Velthoven, T. N. Nguyen, J. Goldy, A. E. Sedeno-Cortes, F. Baftizadeh, D.
686 Bertagnolli, T. Casper, M. Chiang, K. Crichton, S.-L. Ding, O. Fong, E. Garren, A. Glandon, N.
687 W. Gouwens, J. Gray, L. T. Graybuck, M. J. Hawrylycz, D. Hirschstein, M. Kroll, K. Lathia, C.
688 Lee, B. Levi, D. McMillen, S. Mok, T. Pham, Q. Ren, C. Rimorin, N. Shapovalova, J. Sulc, S. M.
689 Sunkin, M. Tieu, A. Torkelson, H. Tung, K. Ward, N. Dee, K. A. Smith, B. Tasic, H. Zeng, A

taxonomy of transcriptomic cell types across the isocortex and hippocampal formation. *Cell* (2021), doi:10.1016/j.cell.2021.04.021.

50. J. Ho, T. Tumkaya, S. Aryal, H. Choi, A. Claridge-Chang, Moving beyond P values: data analysis with estimation graphics. *Nature Methods*. **16** (2019), pp. 565–566.

51. A. R. Nectow, M. V. Moya, M. I. Ekstrand, A. Mousa, K. L. McGuire, C. E. Sferrazza, B. C. Field, G. S. Rabinowitz, K. Sawicka, Y. Liang, J. M. Friedman, N. Heintz, E. F. Schmidt, Rapid Molecular Profiling of Defined Cell Types Using Viral TRAP. *Cell Reports*. **19**, 655–667 (2017).

52. L. Huang, P. Ledochowitsch, U. Knoblich, J. Lecoq, G. J. Murphy, R. C. Reid, S. E. J. de Vries, C. Koch, H. Zeng, M. A. Buice, J. Waters, L. Li, Relationship between simultaneously recorded spiking activity and fluorescence signal in gcamp6 transgenic mice. *Elife*. **10** (2021), doi:10.7554/ELIFE.51675.

53. C. Grienberger, A. Konnerth, Imaging Calcium in Neurons. *Neuron*. **73**, 862–885 (2012).

54. J. C. Webster, M. M. Francis, J. K. Porter, G. Robinson, C. Stokes, B. Horenstein, R. L. Papke, Antagonist activities of mecamylamine and nicotine show reciprocal dependence on beta subunit sequence in the second transmembrane domain. *British Journal of Pharmacology*. **127**, 1337–1348 (1999).

55. R. L. Papke, C. Stokes, P. Muldoon, M. Imad Damaj, Similar activity of mecamylamine stereoisomers in vitro and in vivo. *Eur J Pharmacol*. **720**, 264 (2013).

56. B. Tasic, V. Menon, T. N. Nguyen, T. K. Kim, T. Jarsky, Z. Yao, B. Levi, L. T. Gray, S. A. Sorensen, T. Dolbeare, D. Bertagnolli, J. Goldy, N. Shapovalova, S. Parry, C. Lee, K. Smith, A. Bernard, L. Madisen, S. M. Sunkin, M. Hawrylycz, C. Koch, H. Zeng, Adult mouse cortical cell taxonomy revealed by single cell transcriptomics. *Nature Neuroscience*. **19**, 335–346 (2016).

57. D. Yang, R. Günter, G. Qi, G. Radnikow, D. Feldmeyer, Muscarinic and Nicotinic Modulation of Neocortical Layer 6A Synaptic Microcircuits Is Cooperative and Cell-Specific. *Cerebral Cortex*. **30**, 3528–3542 (2020).

58. F. Ghezzi, A. Marques-Smith, P. G. Anastasiades, D. Lyngholm, C. Vagnoni, A. Rowett, G. Parameswaran, A. Hoerder-Suabedissen, Y. Nakagawa, Z. Molnar, S. J. B. Butt, Non-canonical role for lpar1-egfp subplate neurons in early postnatal mouse somatosensory cortex. *Elife*. **10** (2021), doi:10.7554/ELIFE.60810.

59. J. M. Wess, A. Isaiah, P. V. Watkins, P. O. Kanold, Subplate neurons are the first cortical neurons to respond to sensory stimuli. *Proc Natl Acad Sci U S A*. **114**, 12602–12607 (2017).

60. V. Ochoa, A. A. George, R. Nishi, P. Whiteaker, The prototoxin LYPD6B modulates heteromeric a3β4-containing nicotinic acetylcholine receptors, but not α7 homomers. *The FASEB Journal*. **30**, 1109–1119 (2016).

61. A. B. Tekinay, Y. Nong, J. M. Miwa, I. Lieberam, I. Ibanez-Tallon, P. Greengard, N. Heintz, A role for LYNX2 in anxiety-related behavior. *Proc Natl Acad Sci U S A*. **106**, 4477 (2009).

62. J. Krjukova, T. Holmqvist, A. S. Danis, K. E. O. Åkerman, J. P. Kukkonen, Phospholipase C activator m-3M3FBS affects Ca2+ homeostasis independently of phospholipase C activation. *British Journal of Pharmacology*. **143**, 3–7 (2004).

63. R. M. Sturgeon, N. S. Magoski, A Closely Associated Phospholipase C Regulates Cation Channel Function through Phosphoinositide Hydrolysis. *Journal of Neuroscience*. **38**, 7622–7634 (2018).

64. L. F. Horowitz, W. Hirdes, B.-C. Suh, D. W. Hilgemann, K. Mackie, B. Hille, Phospholipase C in Living Cells Activation, Inhibition, Ca2+ Requirement, and Regulation of M Current. *Journal of General Physiology*. **126**, 243–262 (2005).

65. A. Kuryatov, J. Onksen, J. Lindstrom, Roles of accessory subunits in α4β2* nicotinic receptors. *Molecular Pharmacology* (2008), doi:10.1124/mol.108.046789.

66. W. M. Howe, J. L. Brooks, P. L. Tierney, J. Pang, A. Rossi, D. Young, K. Dlugolenski, E. Guillmette, M. Roy, K. Hales, R. Kozak, α5 nAChR modulation of the prefrontal cortex makes attention resilient. *Brain Structure and Function*. **223**, 1035–1047 (2018).

67. W. Guo, A. R. Clause, A. Barth-Maron, D. B. P. Correspondence, D. B. Polley, A Corticothalamic Circuit for Dynamic Switching between Feature Detection and Discrimination Article A Corticothalamic Circuit for Dynamic Switching between Feature Detection and Discrimination. *Neuron*. **95**, 180–194 (2017).

68. D. P. Collins, P. G. Anastasiades, J. J. Marlin, A. G. Carter, Reciprocal Circuits Linking the Prefrontal Cortex with Dorsal and Ventral Thalamic Nuclei. *Neuron* (2018), doi:10.1016/j.neuron.2018.03.024.

69. M. K. Tian, E. F. Schmidt, E. K. Lambe, *eNeuro*, in press, doi:10.1523/ENEURO.0269-16.2016.

70. D. S. Bortone, S. R. Olsen, M. Scanziani, Translaminar inhibitory cells recruited by layer 6 corticothalamic neurons suppress visual cortex. *Neuron*. **82**, 474–485 (2014).

71. J. Kim, C. J. Matney, A. Blankenship, S. Hestrin, S. P. Brown, Layer 6 Corticothalamic Neurons Activate a Cortical Output Layer, Layer 5a. *Journal of Neuroscience*. **34**, 9656–9664 (2014).

72. S. C. Sundberg, S. H. Lindström, G. M. Sanchez, B. Granseth, Cre-expressing neurons in visual cortex of Ntsr1-Cre GN220 mice are corticothalamic and are depolarized by acetylcholine. *Journal of Comparative Neurology*. **526**, 120–132 (2018).

73. Z. Molnár, H. J. Luhmann, P. O. Kanold, Transient cortical circuits match spontaneous and sensory-driven activity during development. *Science*. **370** (2020), doi:10.1126/science.abb2153.

74. M. Marx, G. Qi, I. L. Hanganu-Opatz, W. Kilb, H. J. Luhmann, D. Feldmeyer, Neocortical Layer 6B as a Remnant of the Subplate - A Morphological Comparison. *Cerebral Cortex*. **27**, 1011–1026 (2017).

75. N. Mechawar, L. Descarries, The cholinergic innervation develops early and rapidly in the rat cerebral cortex: a quantitative immunocytochemical study. *Neuroscience*. **108**, 555–567 (2001).

76. A. Hoerder-Suabedissen, W. Z. Wang, S. Lee, K. E. Davies, A. M. Goffinet, S. Rakić, J. Parnavelas, K. Reim, M. Nicolić, O. Paulsen, Z. Molnár, Novel Markers Reveal Subpopulations of Subplate Neurons in the Murine Cerebral Cortex. *Cerebral Cortex*. **19**, 1738–1750 (2009).

77. S. Y. X. Tiong, Y. Oka, T. Sasaki, M. Taniguchi, M. Doi, H. Akiyama, M. Sato, Kcnab1 is expressed in subplate neurons with unilateral long-range inter-areal projections. *Frontiers in Neuroanatomy*. **13**, 39 (2019).

78. A. Hoerder-Suabedissen, F. M. Oeschger, M. L. Krishnan, T. G. Belgard, W. Z. Wang, S. Lee, C. Webber, E. Petretto, A. D. Edwards, Z. Molnár, Expression profiling of mouse subplate reveals a dynamic gene network and disease association with autism and schizophrenia. *Proc Natl Acad Sci U S A*. **110**, 3555–3560 (2013).

79. T. A. Zolnik, J. Ledderose, M. Toumazou, T. Trimbuch, T. Oram, C. Rosenmund, B. J. Eickholt, R. N. S. Sachdev, M. E. Larkum, Layer 6b Is Driven by Intracortical Long-Range Projection Neurons. *Cell Reports*. **30**, 3492-3505.e5 (2020).

80. R. Egger, R. T. Narayanan, J. M. Guest, A. Bast, D. Udvary, L. F. Messore, S. Das, C. P. J. de Kock, M. Oberlaender, Cortical Output Is Gated by Horizontally Projecting Neurons in the Deep Layers. *Neuron*. **105**, 122-137.e8 (2020).

81. Y. Sherafat, E. Chen, V. Lallai, M. Bautista, J. P. Fowler, Y. C. Chen, J. Miwa, C. D. Fowler, Differential Expression Patterns of Lynx Proteins and Involvement of Lynx1 in Prepulse Inhibition. *Frontiers in Behavioral Neuroscience*. **15** (2021), doi:10.3389/FNBEH.2021.703748.

82. W. A. Nichols, B. J. Henderson, C. Yu, R. L. Parker, C. I. Richards, H. A. Lester, J. M. Miwa, Lynx1 Shifts α4β2 Nicotinic Receptor Subunit Stoichiometry by Affecting Assembly in the Endoplasmic Reticulum *. *Journal of Biological Chemistry*. **289**, 31423–31432 (2014).

83. J. M. Miwa, I. Ibañez-Tallon, G. W. Crabtree, R. Sánchez, A. Šali, L. W. Role, N. Heintz, lynx1, an Endogenous Toxin-like Modulator of Nicotinic Acetylcholine Receptors in the Mammalian CNS. *Neuron*. **23**, 105–114 (1999).

84. I. Ibañez-Tallon, J. M. Miwa, H. L. Wang, N. C. Adams, G. W. Crabtree, S. M. Sine, N. Heintz, Novel modulation of neuronal nicotinic acetylcholine receptors by association with the endogenous prototoxin lynx1. *Neuron*. **33**, 893–903 (2002).

85. H. Morishita, J. M. Miwa, N. Heintz, T. K. Hensch, Lynx1, a Cholinergic Brake, Limits Plasticity in Adult Visual Cortex. *Science (1979)*. **330**, 1238–1240 (2010).

86. M. S. Thomsen, M. Arvaniti, M. M. Jensen, M. A. Shulepko, D. A. Dolgikh, L. H. Pinborg, W. Härtig, E. N. Lyukmanova, J. D. Mikkelsen, Lynx1 and Aβ1–42 bind competitively to multiple nicotinic acetylcholine receptor subtypes. *Neurobiology of Aging*. **46**, 13–21 (2016).

87. Z. O. Shenkarev, M. A. Shulepko, M. L. Bychkov, D. S. Kulbatskii, O. V. Shlepova, N. A. Vasilyeva, A. A. Andreev-Andrievskiy, A. S. Popova, E. A. Lagereva, E. V. Loktyushov, S. G. Koshelev, M. S. Thomsen, D. A. Dolgikh, S. A. Kozlov, P. M. Balaban, M. P. Kirpichnikov, E. N. Lyukmanova, Water-soluble variant of human Lynx1 positively modulates synaptic plasticity and ameliorates cognitive impairment associated with α7-nAChR dysfunction. *Journal of Neurochemistry*. **155**, 45–61 (2020).

88. M. Sadahiro, M. P. Demars, P. Burman, P. Yevoo, A. Zimmer, H. Morishita, Activation of Somatostatin Interneurons by Nicotinic Modulator Lypd6 Enhances Plasticity and Functional Recovery in the Adult Mouse Visual Cortex. *Journal of Neuroscience*. **40**, 5214–5227 (2020).

89. G. Paxinos, K. Franklin, *Paxinos and Franklin's the Mouse Brain in Stereotaxic Coordinates* (2004).

Figure legends

Figure 1. Chrna5 expression identifies a distinct population of prefrontal neurons with stronger and faster-onset optogenetic cholinergic responses. A, Breeding scheme to obtain triple transgenic *Chrna5*-Cre$^{/+}$Ai14$^{/+}$ChAT-ChR2$^{/+}$ mice expressing tdTomato in *Chrna5*-expressing (Chrna5+) neurons and Channelrhodopsin 2 in cholinergic axons. **B,** Top- Schematic of coronal mPFC slice with region of interest, adapted from (*89*). Bottom- two photon imaging (3D projection) of tdTomato-labeled Chrna5+ neurons and EYFP-labeled cholinergic axons in layer 6 of mPFC slices. **C,** IRDIC (left) and widefield fluorescence (TRITC, right) images of tdTomato labeled Chrna5+ and unlabeled layer 6 neurons during whole cell patch clamp electrophysiology. Clearing induced by the pipette is visible. **D,** Average light-evoked endogenous cholinergic response of labeled Chrna5+ vs neighbouring unlabeled Chrna5- neurons. Dotted lines are the slope of the response onset. (Inset) Individual responses are zoomed in to show the onset. **E-F,** Bar graph comparing (E) Rising slope and (F) Peak current of endogenous cholinergic responses between labeled Chrna5+ neurons (n = 24 cells) and unlabeled Chrna5- neurons (n = 15 cells, 4 mice). *P < 0.05, Unpaired t-test. Top) **G,** (Top) Breeding scheme to obtain triple transgenic *Chrna5*-Cre$^{/+}$Ai14$^{/+}$*Syt6*-EGFP$^{/+}$ mice expressing tdTomato in Chrna5+ neurons and EGFP in Syt6+ neurons (Bottom) Confocal imaging in mPFC slices shows Chrna5+ and Syt6+ neurons distributed in layer 6. **H-I,** Confocal (H) and two-photon imaging (I) reveal three populations of neurons: exclusively Chrna5+ neurons which do not express *Syt6*, overlapping Chrna5+Syt6+ neurons which express both markers, and exclusively Syt6+ neurons which do not express *Chrna5*. **J,** Left- Graph quantifies the percentage of each cell type with respect to all labeled cells per sample. Right- Average proportions of Chrna5+, Chrna5+Syt6+ and Syt6+ neurons.

Figure 2. Calcium imaging in Chrna5+ and Syt6+ populations reveals a distinct subset of Chrna5+ neurons with resilient nicotinic responses. A, Top: Two photon calcium imaging in prefrontal brain slices from *Chrna5*-Cre$^{/+}$Ai96$^{/+}$ (left) and *Syt6*-Cre$^{/+}$Ai96$^{/+}$ mice (right) showing acetylcholine-evoked GCaMP6s responses in Chrna5+ and Syt6+ neurons respectively (scale 50 µm). Bottom: Acetylcholine-evoked GCaMP6s signals were sequentially recorded after application of competitive nicotinic antagonist DHBE and addition of muscarinic antagonist atropine (scale 10 µm). **B,** Normalized fluorescence signal **(**ΔF by F) evoked by acetylcholine in individual Chrna5+ and Syt6+ neurons in a brain slice at baseline (left), after DHBE (middle), and after DHBE + Atropine (right). (Inset, average response and standard deviation. Scale: same as main figure). **C-D i,** Boxplot shows the percentage of response remaining after the application of (C) DHBE and (D) DHBE + Atropine (Inset shows the same boxplot with a restricted y-axis). + denote respective means. Responses were quantified by the area under the ΔF/F curve (n = 71 neurons, 6 mice for Chrna5+, and 112 neurons, 7 mice for Syt6+, ****P <10^{-4}, Mann-Whitney test). **C-D ii,** Cumulative frequency distribution of the percentage response remaining after **(**C) DHBE and (D) DHBE + Atropine (P < 10^{-4}, Kolmogorov-Smirnov test). **C-D iii,** Proportion of cells showing zero and non-zero responses after (C) DHBE and (D) DHBE + Atropine (P < 10^{-4} for both C & D, Fisher's exact test). **E,** Current clamp responses evoked by 1mM acetylcholine (15s) in fluorescently labeled Chrna5+ and Syt6+ layer 6 neurons patched in mPFC slices from mice *Chrna5*-Cre$^{/+}$ Ai14$^{/+}$ and *Syt6*-Cre$^{/+}$Ai14$^{/+}$ or *Syt6*-EGFP mice respectively. **F,** Peak spike frequency in Chrna5+ and Syt6+ neurons evoked by acetylcholine (left), in the presence of

competitive nicotinic antagonist DHBE and atropine (middle). Residual response remaining after DHBE + Atropine in a distinct subset of Chrna5+ neurons is blocked by non-competitive nicotinic antagonist mecamylamine (right). (**$P < 0.01$, *$P < 0.05$, unpaired t-test).

Figure 3. Single cell transcriptomic analysis reveals Chrna5+ subset to span subplate neuron populations with differential expression of lynx prototoxin genes A, Single cell-RNAseq data for 2422 L5-6 glutamatergic neurons in the anterior cingulate cortex (ACA, shown in schematic on the left) was obtained from publicly available datasets (Allen Institute, SMARTSeq ACA and MOP (2018)). Right- Scatter plot showing *Chrna5* vs *Syt6* expression in $\log_{10}$ (Copies per million) for each neuron, with the frequency distribution shown on the corresponding axes. Neurons were classified into Chrna5+, Chrna5+Syt6+ and Syt6+ groups based on their expression of *Chrna5* and *Syt6* genes. Cells which expressed neither gene were excluded from subsequent analyses. **B**, The major neuronal subclasses within Chrna5+, Chrna5+Syt6+ and Syt6+ groups is indicated by the colorbar on top. NP- Near projecting, CT- Corticothalamic. Heatmap shows expression of subplate and corticothalamic marker genes in each cell in all 3 groups. **C,** Dotplot shows summary of subplate and corticothalamic marker expression in Chrna5+, Chrna5+Syt6+ and Syt6+ groups. Dot size indicates the percentage of cells within each group expressing that gene, color of the dot indicates average expression level relative to other groups. Chrna5+ neurons highly express multiple subplate marker genes, but not corticothalamic markers. **D**, Violin plots show expression of Lynx prototoxins *Ly6g6e*, *Lypd1* (Lynx2) and *Lypd6b* which show highest fold-change between Chrna5+ and Chrna5+Syt6+ neurons. **E,** Dotplot shows expression of major genes known to modulate cholinergic function, including nicotinic, muscarinic subunits, acetylcholinesterase, and lynx prototoxins in Chrna5+, Chrna5+Syt6+ and Syt6+ neurons. Genes are ordered by decreasing fold change in expression. Dot size indicates the percentage of cells within each group expressing that gene, color of the dot indicates average expression level relative to other groups. Fold change of all the genes shown in this dotplot are listed in Supplemetary table 3

Figure 4. Regulation of optogenetic nicotinic responses by endogenous GPI-anchored lynxes and cell type specific effects of recombinant Ly6g6e. A, Schematic of nicotinic receptor environment showing endogenous GPI-anchored lynxes exerting positive and negative modulation of nicotinic receptors. The compound m-3M3FBS activates PLC, cleaving the GPI anchor and perturbing lynx-mediated modulation of nicotinic responses. **B,** Optogenetic nicotinic responses in prefrontal deep-layer pyramidal neurons from ChAT-ChR2 mice before and after treatment with m-3M3FBS (5 min). **C,** PLC activation significantly increased the rising slope of optogenetic nicotinic responses. Change in **D,** Rising slope and **E,** Area of nicotinic response in control and after PLC activation. (*$P < 0.05$, **$P < 0.01$, Wilcoxon matched-pairs test). **E,** IRDIC (left) and widefield fluorescence (right) images of tdTomato labeled Chrna5+ (top) and Syt6+ (bottom) deep layer neurons during whole-cell patch clamp electrophysiology in *Chrna5*-Cre$^{/+}$Ai14$^{/+}$ChAT-ChR2$^{/+}$ and *Syt6*-Cre$^{/+}$Ai14$^{/+}$ChAT-ChR2$^{/+}$ mouse brain slices respectively. **G,** Schematic summarising predicted and observed effects of recombinant water-soluble ly6g6e on Chrna5+ and Syt6+ neuronal nicotinic receptors. **G,** Optogenetic nicotinic responses are reduced in amplitude following 10 minute application of soluble ly6g6e in Syt6+ but not Chrna5+ neurons. Change in peak current (I) and area of the nicotinic response (**J**) of Chrna5+ vs Syt6+ neurons (*$P < 0.05$, ** $P < 0.01$, Unpaired t-test)

Figure 5. Graphical summary. Deep-layer pyramidal neurons can be divided into three groups (Chrna5+, Chrna5+Syt6+, Syt6+) by their expression of *Chrna5* and *Syt6* genes. The subset of *Chrna5*-expressing neurons without *Syt6* expression are molecularly distinct and comprise of subplate neurons, whereas *Syt6*-expressing neurons are of the corticothalamic subtype. Nicotinic receptors in these neurons are under complex regulation by endogenous lynx prototoxins. Inhibitory prototoxin gene *Lynx1* is expressed uniformly in all neurons, whereas Chrna5+ subplate neurons additionally have specific expression of *Ly6g6e*, *Lypd1* and *Lypd6b* prototoxin genes. These Chrna5+ subplate neurons show enhanced α5 subunit nicotinic receptor-mediated cholinergic responses that are differently modulated by specific lynx prototoxins.

Supplementary materials

Supplementary video 1 & 2: Videos show **(1)** Chrna5+ neurons in mPFC slices from *Chrna5*-Cre$^{/+}$Ai96$^{/+}$ mice and **(2)** Syt6+ neurons from *Syt6*-Cre$^{/+}$Ai96$^{/+}$ mice responding to exogenous application of 1mM acetylcholine with an increase in GCaMP6s fluorescence signal.

Supplementary table 1: Intrinsic electrophysiological properties of Chrna5+ and Chrna5- unlabeled deep-layer neurons in *Chrna5*-Cre$^{/+}$Ai14$^{/+}$ChAT-ChR2$^{/+}$ mice.

Supplementary table 2: Intrinsic electrophysiological properties of Chrna5+ and Syt6+ deep-layer neurons.

Supplementary table 3: Table comparing expression of major genes modulating postsynaptic cholinergic responses in Chrna5+ and Chrna5+Syt6+ neurons.

Supplementary table 4. Table of all differentially expressed genes between Chrna5+ and Chrna5+Syt6+ neurons with adjusted p value < 0.05

Figures and Tables

Figure 1

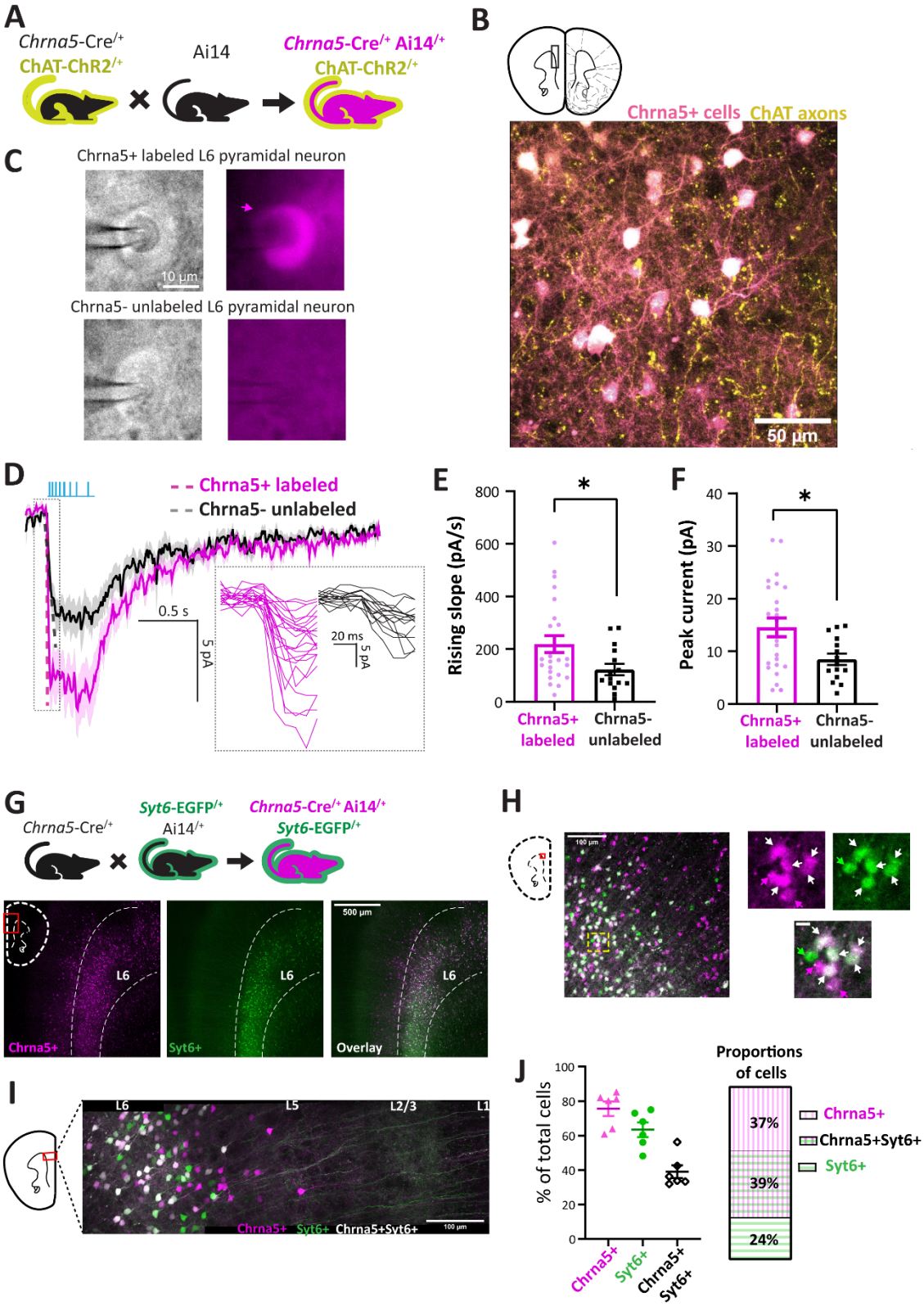

Figure 2

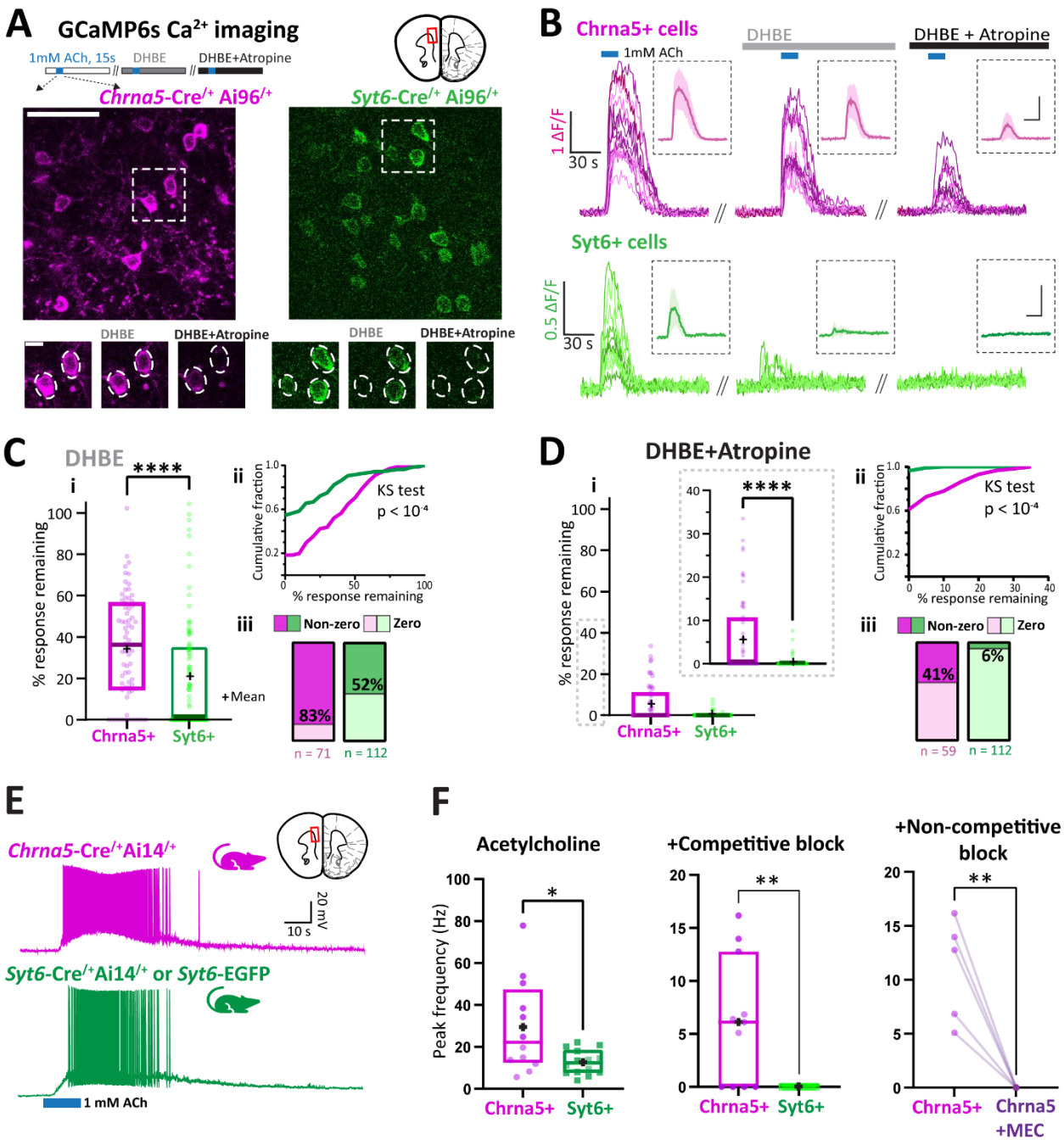

Figure 3

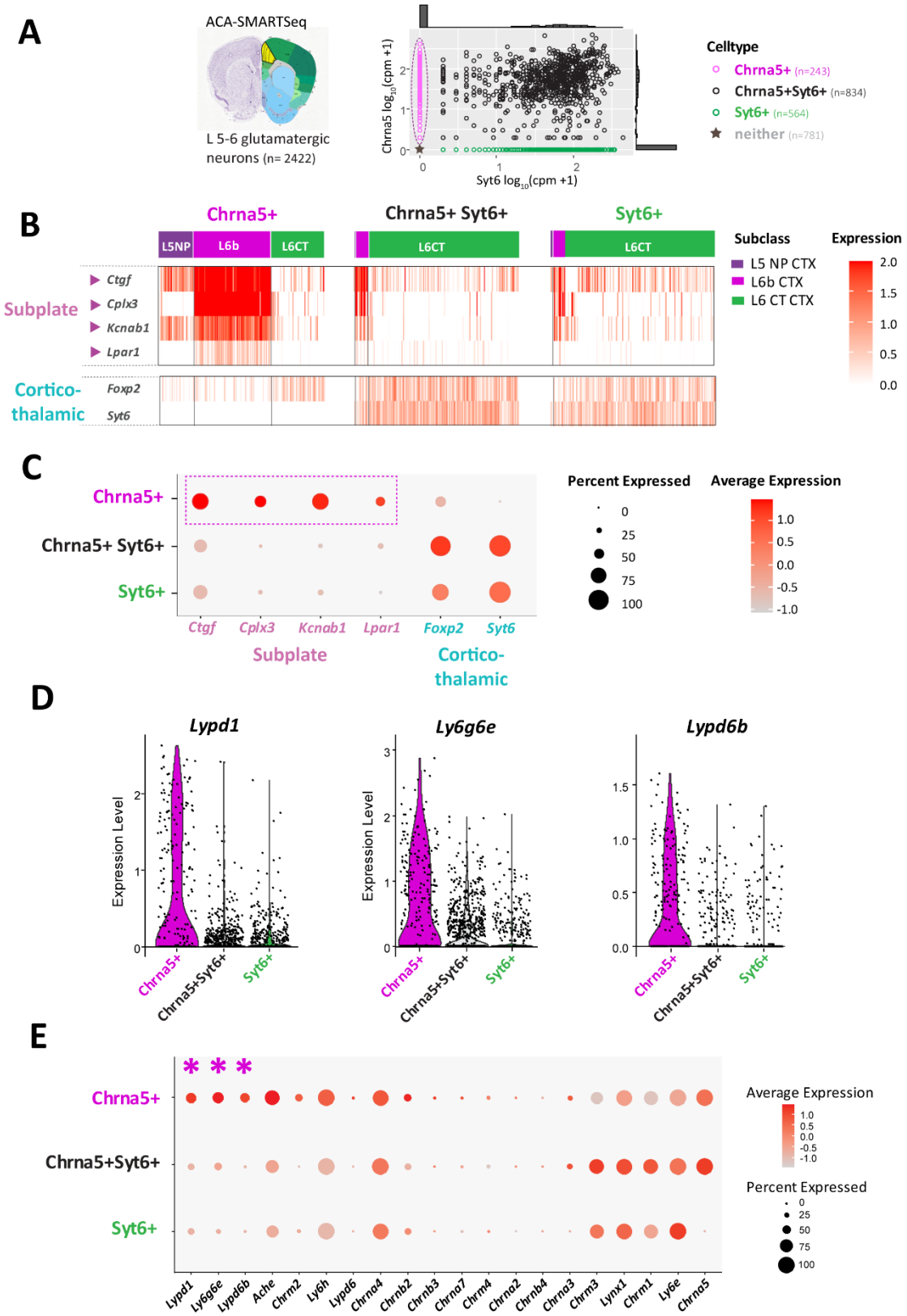

Figure 4

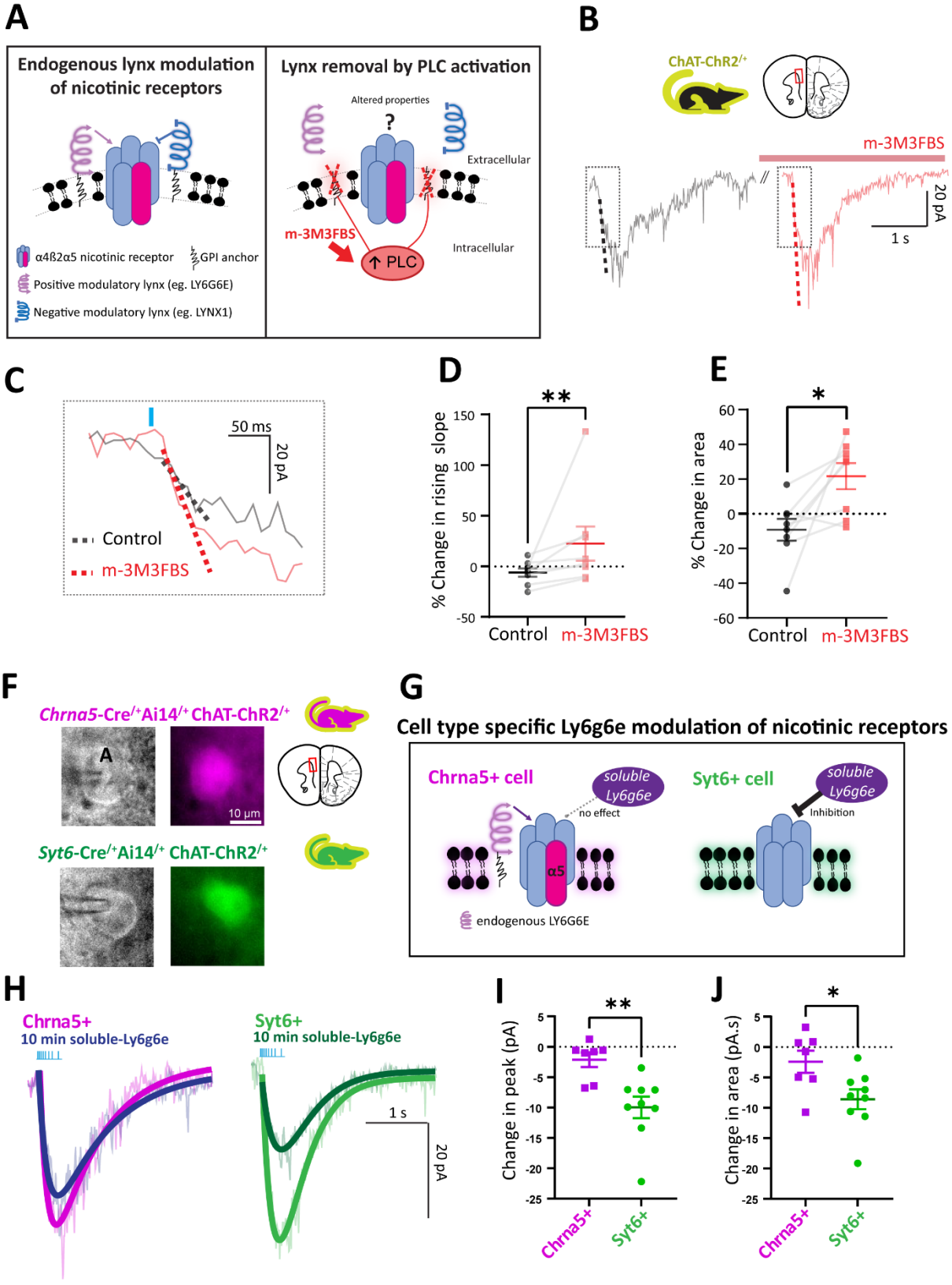

Figure 5

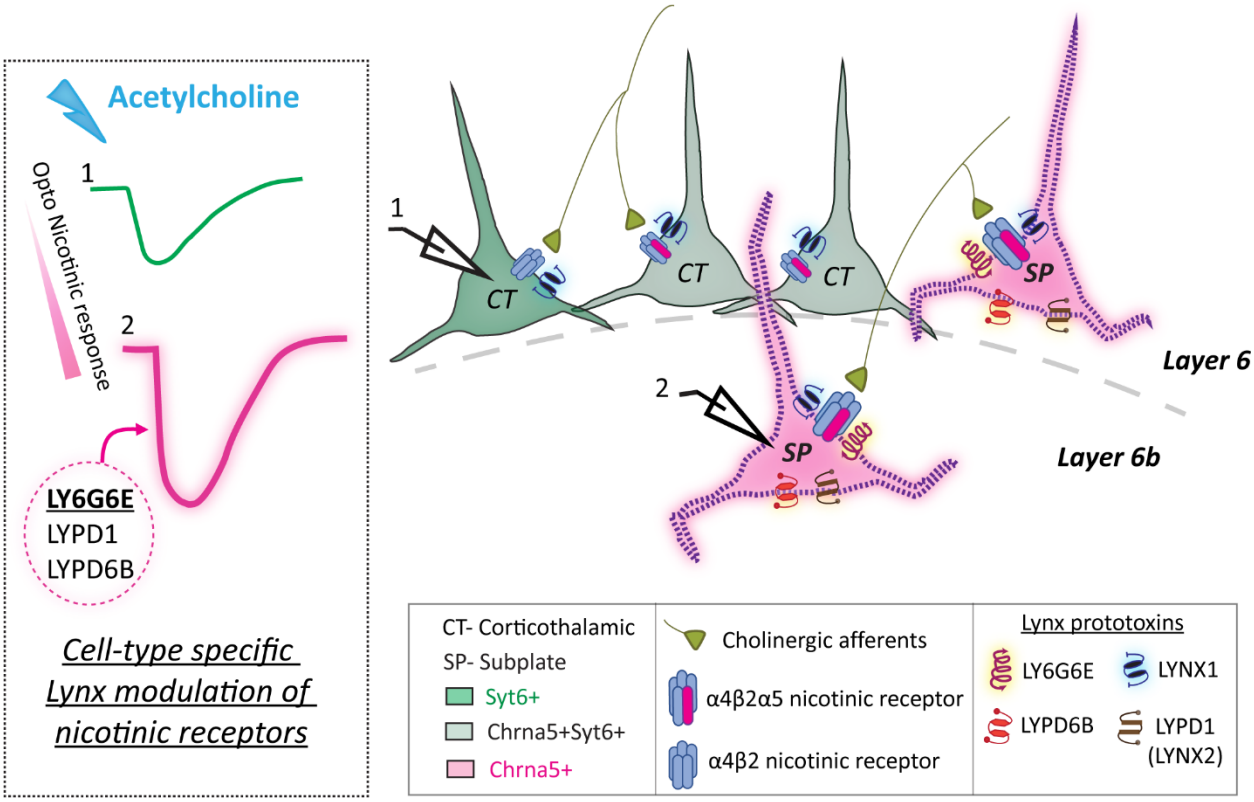

Table 1

Genes	P value	Chrna5+ cells %	Chrna5+Syt6+ cells %	Adjusted P value	Fold change (Chrna5+/ Chrna5+Syt6)
***Cplx3**	1.16E-43	0.535	0.149	3.37E-39	5.69
***Ctgf**	1.60E-28	0.77	0.568	4.65E-24	3.81
Ptn	3.68E-28	0.864	0.758	1.07E-23	3.60
***Tmem163**	2.12E-44	0.51	0.129	6.16E-40	2.58
Lypd1	3.40E-23	0.593	0.381	9.88E-19	2.55
***Kcnab1**	3.81E-74	0.741	0.191	1.11E-69	2.51
Serpini1	1.54E-50	1	0.993	4.49E-46	2.50
Hpcal1	2.48E-27	0.658	0.39	7.20E-23	2.47
Nrsn2	1.89E-30	0.864	0.767	5.50E-26	2.28
Ntm	1.83E-56	0.889	0.59	5.31E-52	2.21
Tshz2	2.82E-16	0.535	0.327	8.20E-12	2.17
Etv1	5.70E-16	0.395	0.186	1.66E-11	2.16
Rcn2	5.18E-46	0.996	0.984	1.51E-41	2.14
Olfm3	1.67E-44	0.897	0.716	4.86E-40	2.11
Crtac1	5.50E-46	0.728	0.347	1.60E-41	2.04
***Ly6g6e**	2.13E-25	0.671	0.434	6.20E-21	2.03
Adk	6.31E-29	0.922	0.922	1.83E-24	2.00
Trp53i11	2.73E-60	0.724	0.222	7.94E-56	1.93
Cd164	6.72E-18	0.897	0.882	1.95E-13	1.92
Dner	2.35E-45	0.712	0.326	6.82E-41	1.85

Top 20 differentially expressed genes between Chrna5+ and Chrna5+Syt6+ neuron. Top 20 differentially expressed genes determined by the FindMarkers function on Seurat ordered by decreasing fold change. Several known subplate neuron markers (highlighted by *****) are the highest enriched genes in Chrna5+ neurons. All differentially expressed genes are listed in supplementary table 4.